1   *Sulfur Isotope Effects of Dissimilatory Sulfite Reductase*

3   William D. Leavitt[1,2,†*], Alexander S. Bradley[2†], André A. Santos[3],

4   Inês A. C. Pereira[3] and David T. Johnston[1]

6   [1]Department of Earth & Planetary Sciences, Harvard University, Cambridge, MA, USA,

7   [2]Department of Earth and Planetary Sciences, Washington University in St. Louis, MO, USA.

8   [3]Instituto de Tecnologia Química e Biológica António Xavier, Universidade Nova de Lisboa, Oeiras,

9   Portugal

11   *Corresponding author*: wleavitt@eps.wustl.edu

12   [†]Authors contributed equally

14   **Abstract**

15   **The precise interpretation of environmental sulfur isotope records requires a quantitative**
16   **understanding of the biochemical controls on sulfur isotope fractionation by the principle**
17   **isotope-fractionating process within the S cycle, microbial sulfate reduction (MSR). Here we**
18   **provide the only direct observation of the major ($^{34}S/^{32}S$) and minor ($^{33}S/^{32}S$, $^{36}S/^{32}S$) sulfur**
19   **isotope fractionations imparted by a central enzyme in the energy metabolism of sulfate reducers,**
20   **dissimilatory sulfite reductase (DsrAB). Results from in vitro sulfite reduction experiments allow**
21   **us to calculate the in vitro DsrAB isotope effect in $^{34}S/^{32}S$ (hereafter, $^{34}\varepsilon_{DsrAB}$) to be 15.3±2‰, 2σ.**
22   **The accompanying minor isotope effect in ^{33}S, described as $^{33}\lambda_{DsrAB}$, is calculated to be**
23   **0.5150±0.0012, 2σ. These observations facilitate a rigorous evaluation of the isotopic**
24   **fractionation associated with the dissimilatory MSR pathway, as well as of the environmental**
25   **variables that govern the overall magnitude of fractionation by natural communities of sulfate**
26   **reducers. The isotope effect induced by DsrAB upon sulfite reduction is a factor of 0.3 to 0.6 times**
27   **prior indirect estimates, which have ranged from 25 to 53‰ in $^{34}\varepsilon_{DsrAB}$. The minor isotope**
28   **fractionation observed from DsrAB is consistent with a kinetic or equilibrium effect. Our in vitro**
29   **constraints on the magnitude of $^{34}\varepsilon_{DsrAB}$ is similar to the median value of experimental observations**
30   **compiled from all known published work, where $^{34}\varepsilon_{r-p}$ = 16.1‰ (*r* – *p* indicates reactant versus**
31   **product, n = 648). This value closely matches those of MSR operating at high sulfate reduction**
32   **rates in both laboratory chemostat experiments ($^{34}\varepsilon_{SO4-H2S}$ = 17.3±1.5‰) and in modern marine**
33   **sediments ($^{34}\varepsilon_{SO4-H2S}$ = 17.3±3.8‰). Targeting the direct isotopic consequences of a specific**
34   **enzymatic processes is a fundamental step toward a biochemical foundation for reinterpreting the**
35   **biogeochemical and geobiological sulfur isotope records in modern and ancient environments.**

37   **Introduction**

38   Microbial sulfate reduction provides a critical link between Earth's exogenic sulfur, carbon, iron and
39   oxygen cycles (Thode et al., 1961; Canfield, 2001a; Garrels and Lerman, 1981; Holland, 1973). This
40   metabolism is comprised of a set of enzymes working in concert to reduce sulfate (SO_4^{2-}) to sulfide (H_2S)
41   (Pereira et al., 2011; Peck, 1961) (Figure 1). During this transformation, MSR generates $^{34}S/^{32}S$, $^{33}S/^{32}S$,
42       $^{36}S/^{32}S$, $^{18}O/^{16}O$ and $^{17}O/^{16}O$ stable isotope fractionations (Harrison and Thode, 1958; Kaplan and
43   Rittenberg, 1964; Chambers et al., 1975; Kemp and Thode, 1968; Canfield, 2001b; Goldhaber and
44   Kaplan, 1975; Leavitt et al., 2013; Sim et al., 2011b; Fritz et al., 1989), the biochemical source of which is
45   unclear (Chambers and Trudinger, 1979). To construct a biochemically constrained perspective of sulfur
46   isotope fractionations during MSR requires we quantify how material moves through the metabolic
47   network, and gain an understanding of the isotope effect(s) associated with each constituent enzymatic
48   step (Hayes, 2001).

49
50 The enzyme catalyzed reaction network of MSR is represented in Figure 1. Sulfate is first imported into
51 the cytoplasm by a variety of transporters (Cypionka, 1994; Piłsyk and Paszewski, 2009) (Figure 1), and
52 subsequently activated to a high-energy intermediate, adenosine 5'-phosphosulfate (APS). The latter
53 reaction generates pyrophosphate (PPi) at the expense of ATP by the enzyme sulfate-adenylyl
54 transferase (Sat) (Peck, 1962). APS is reduced to sulfite (SO_3^{2-}) through a two-electron transfer by the
55 soluble cytoplasmic enzyme APS oxidoreductase (ApsR) (Peck, 1959), which is linked to energy
56 conservation by the membrane-bound complex QmoABC (Pires et al., 2003). APS reduction is highly
57 reversible, depending on the in vivo or in vitro conditions (Peck, 1960). Sulfite has several potential
58 fates. Sulfite can either be re-oxidized to sulfate (directly or via APS) or further reduced to sulfide by
59 DsrAB with the involvement of DsrC (Oliveira et al., 2008b). A critical step is during the reduction of
60 sulfite when it binds the iron of the siroheme in the DsrAB active site. The subsequent reduction occurs
61 via electron transfer from an adjacent Fe-S cluster (Oliveira et al., 2008a; 2008b; Parey et al., 2010). In
62 vivo, DsrAB has been proposed to generate intermediate valence sulfur, which is then bound to DsrC and
63 converted to sulfide via DsrC/MK (Oliveira et al., 2008b; Venceslau et al., 2013; 2014). Sulfide then
64 leaves the cell by diffusion (as H_2S) or through anion transport (as HS^- or S^{2-}). In instances when DsrC is
65 unavailable (e.g. when DsrAB is pure in vitro) or limiting (e.g. intracellular sulfite is in excess of reduced
66 DsrC), intermediates such as thiosulfate ($S_2O_3^{2-}$) may become important, likely due to the reaction of
67 sulfite with sulfide (in vivo) or the partially reduced sulfur from DsrAB (in vitro) (Drake and Akagi,
68 1976; Chambers and Trudinger, 1975; Drake and Akagi, 1978; Kim and Akagi, 1985; Drake and Akagi,
69 1977). A few examples exist where thiosulfate is a key component in closing S mass balance during in
70 vivo MSR (Sass et al., 1992; Price et al., 2014; Leavitt et al., 2014), and in one instance trithionate is
71 observed ($S_3O_6^{2-}$) (Sass et al., 1992), though it is not clear in this case it is a physiological product. Under
72 these conditions, accumulation and excretion of such compounds as thiosulfate may be important
73 (Bradley et al., 2011). It is within this broader biochemical and physiological context that we examine the
74 isotopic consequences of sulfite reduction by DsrAB, which as outlined above, is central to the
75 biochemistry of dissimilatory sulfate reduction.
76
77 Reduction of sulfite by DsrAB breaks three of the four S-O bonds in the original sulfate (Venceslau et al.,
78 2014). As such, the isotope effect of DsrAB likely plays a significant role in setting the overall
79 fractionations observed from MSR (Harrison and Thode, 1958; Rees, 1973; Brunner and Bernasconi,
80 2005; Farquhar et al., 2003). Measured enzyme-specific isotope effects are lacking for MSR and the S
81 cycle in general. Such information has been transformative for the study of other biogeochemical
82 elements like carbon. For example, experimental work quantifying the $^{13}C/^{12}C$ effect of RuBisCO (Park
83 and Epstein, 1960; Farquhar et al., 1982; Tcherkez et al., 2006), the core enzyme in carbon fixation, has
84 greatly advanced the applicability of carbon isotope biogeochemistry. More specifically, understanding
85 the fractionation associated with RuBisCO allowed greater insight into modern (Hayes, 1993) and
86 ancient (Hayes et al., 1999) carbon cycling, and facilitated a better understanding of primary productivity
87 in the both modern (Laws et al., 1995) and ancient (Pagani et al., 2009) oceans. Similar approaches have
88 also proven greatly informative in studies of methane production (Scheller et al., 2013), nitrate
89 assimilation (Karsh et al., 2012), and nitrogen fixation (Sra et al., 2004). With these studies as a guide,
90 we look to further unlock the sulfur cycle through targeting a key microbial sulfate reduction enzyme,
91 DsrAB.
92
93 To close the knowledge gap between whole-cell observations and enzyme-catalyzed reactions, as well as
94 to turn natural isotope records into catalogues of environmental information, we conduct the first
95 enzyme-specific sulfur isotope experiments. Here we report the sulfur isotope fractionation factors
96 associated with in vitro sulfite reduction by the dissimilatory sulfite reductase enzyme (DsrAB). Using
97 these results and a new mathematical model, we are able to place improved constraints on the root of

98   sulfur isotope fractionation during MSR. This refines our understanding of the predominant biological
99   process responsible for generating environmental S isotope records throughout geological history.
100
101   **Experimental Methods Summary**
102   We conducted a series of closed system in vitro sulfite reduction experiments with purified DsrAB from
103   *Desulfovibrio vulgaris* str. Hildenborough (DSM 644) and *Archaeoglobus fulgidus*. These enzymes are
104   structurally similar and evolutionarily related (Parey et al., 2013), and we chose them to attempt to
105   determine conservation of isotope fractionation in *D. vulgaris* and *A. fulgidus* DsrAB. The complete
106   isolation and purification details are available in the Appendix.
107
108   DsrAB experiments were conducted in vitro under strictly anoxic conditions with H_2, [NiFe]
109   hydrogenase, and methyl viologen as the electron donation system. Key considerations in experimental
110   design are: (i) to provide enough sulfur at each time point for isotopic characterization of residual
111   reactant and products; (ii) to provide the proper reaction conditions to allow for optimal DsrAB activity
112   (pH = 7.1, T = 20° or 31°C); (iii) to ensure hydrogenase activity is not inhibited by the experimental pH
113   (optimum at pH 7.5, activity significantly depleted below pH 6.5, so we chose pH 7.1, to account for
114   optima of both DsrAB and [NiFe]-hydrogenase); and finally (iv) to ensure the sulfite to hydrogen ratio
115   favors sulfite reduction. Experiments setup is detailed in the Appendix.
116
117   Each experiment was performed in duplicate and sampled as sulfite was consumed (reaction progress
118   tracked as f_{SO3}, equivalent to the fraction of remaining sulfite). The reaction consumed sulfite to form
119   products thiosulfate and trithionate, with no detectable sulfide. Thiosulfate and trithionate
120   concentrations were quantified following published cyanolysis protocols (Kelly and Wood, 1994), where
121   we used a modified 'Fuschin' method (Grant, 1947) to quantify sulfite and a modified Cline method
122   (Cline, 1969) to measure sulfide. All quantification and experimental methods are fully detailed in the
123   Appendix. In addition to concentrations, we measured the major and minor sulfur isotopic compositions
124   of three operationally defined and precipitated pools: sulfite (both initial and residual reactant), product
125   sulfonate (from trithionate or thiosulfate) and the 'reduced sulfur' reservoirs (central and terminal sulfurs
126   in trithionate and thiosulfate, respectively). Complete IUPAC definitions of each S reservoir, along with
127   all isotopic measurement methods and error propagation calculations are fully articulated in the
128   Appendix.
129
130   **Isotope Notation**
131   The variability in ^{34}S of a measured pool is reported in standard delta notation (for instance $\delta^{34}S$, in ‰
132   units), where $^{34}S/^{32}S$ of the sample is the relative difference from a standard (Hayes, 1983), and is
133   reported as the isotopic offset between two measured pools of sulfur, $^{34}\varepsilon$ ($=10^3 \times (^{34}\alpha - 1)$), still in ‰ units.
134   Fractionation factors (α's and associated ε's) are annotated with a subscript to denote the process of
135   interest or pools being related, such as $^{34}\varepsilon_{DsrAB}$, $^{34}\varepsilon_{MSR}$, $^{34}\varepsilon_{r-p}$ or $^{34}\varepsilon_{SO4-H2S}$. The same nomenclature
136   convention is followed when a minor isotope, ^{33}S, is included. The only exception is the addition of one
137   new term, $^{33}\lambda$, which is approximately the slope of a line on a plot of $\delta^{33}S$ versus $\delta^{34}S$ (Farquhar et al.,
138   2003; Miller, 2002), but can be simply interpreted as a measure of mass-dependent minor isotope
139   fractionation. Mathematical definitions are provided below.
140
141   **Fractionation modeling**
142
143   Calculation of the isotopic fractionation imposed by the reduction of sulfite through DsrAB requires
144   tracking the concentration of the reactant, accumulation of the products, and determining the isotopic
145   composition of all as the reaction progressed. This necessitates the application of a closed-system model
146   in order to calculate fractionation factors. Determining the intrinsic isotope effect associated with a

147 closed system reaction can be approached in a number of ways. Normally, in a system where one reactant
148 is consumed in order to generate a single product, a Rayleigh model is employed (Mariotti et al., 1981;
149 Nakai and Jensen, 1964). This approach assumes that the reaction of interest is unidirectional, generates
150 only one product, and that the fractionation factor is invariant throughout the reaction. In this case, the
151 isotope effect is calculated as a function of the isotope ratio, R, of the starting composition (R_{ao}) and
152 evolving product pool (R_p, defined below), equal to the mass balance on sulfite:
153

154
$$\alpha_{total} = \frac{\ln\left(\frac{R_p}{R_{a0}}(f-1)+1\right)}{\ln(f)}. \qquad \text{(Equation 1)}$$

155
156 In this solution, f tracks the fractional amount of reactant remaining (SO_3^{2-}). For our experiments, we
157 define f_{SO3}:

158
$$f_{SO_3} = \frac{[SO_3^{2-}]_t}{[SO_3^{2-}]_0}. \qquad \text{(Equation 2)}$$

159
160 In the specific case of our experiments and the reduction of sulfite by DsrAB, however, the standard
161 closed-system isotope distillation models (equation 1) requires expansion. Recall that the in vitro
162 reaction involves the accumulation of two products (trithionate and thiosulfate). Each of these products
163 further contains sulfur moieties in more than one oxidation state (Kobayashi et al., 1974; Drake and
164 Akagi, 1977; 1978; Suh and Akagi, 1969; Drake and Akagi, 1976). This means that, rather than R_p being
165 the isotope composition of a single product pool, we define it as the mass-weighted sum of the oxidized
166 (R_{ox}) and reduced (R_{red}) products in trithionate and thiosulfate:
167

168
$$R_p = \left[\frac{1}{2}j + \frac{1}{3}(1-j)\right]R_{red} + \left[\frac{1}{2}j + \frac{2}{3}(1-j)\right]R_{ox}. \qquad \text{(Equation 3)}$$

169 Here the reduced and oxidized pools are the operationally defined reservoirs discussed above. In the
170 mass balance accounting equation we introduce a term to quantify the ratio of products, j (Figure 2).
171 The concentrations of sulfite, trithionate, and thiosulfate were measured at each time-point, ensuring the
172 closure of mass balance and validating the use of a relative mass term. The j term is thus the fraction of
173 products residing in thiosulfate:

174
$$j = \frac{2[S_2O_3^{2-}]_t}{2[S_2O_3^{2-}]_t + 3[S_3O_6^{2-}]_t}. \qquad \text{(Equation 4)}$$

175
176 For isotopic measurements we quantitatively separated the oxidized moieties from trithionate and
177 thiosulfate from the partially reduced moieties of both products. There were no available methods to
178 separate trithionate and thiosulfate and isolate each S site within those products (a target for future
179 work). We then measured the isotopic compositions of the pooled oxidized and pooled reduced
180 products. As the goal is to identify the fractionation between the residual sulfite and either the oxidized
181 ($^{3x}\alpha_{ox}$) or reduced ($^{3x}\alpha_{red}$) moieties in trithionate and thiosulfate, we present the general equation, ($^{3x}\alpha_z$):
182

183
$$\alpha_z = \frac{R_z}{R_{a0}}\frac{\alpha_{total}}{(f^{\alpha_{total}-1})}(f-1), \qquad \text{(Equation 5)}$$

184
185 where z is either ox or red. This solution is then translated into standard $^{3x}\varepsilon$ notation. Fractionation
186 factors are then related in triple isotope space with:
187

188
$$^{3x}\lambda = \frac{\ln(^{3x}\alpha)}{\ln(^{34}\alpha)}, \qquad \text{(Equation 6)}$$

189

190 a term which finds common application in mass-dependent studies (Young et al., 2002; Farquhar et al.,
191 2003). Finally, we note the models assumptions: 1) sulfite and its isomers carry the same isotopic
192 composition as each other, 2) the isotopic composition of the sulfonate groups (in trithionate and
193 thiosulfate) are isotopically identical, and 3) similar to 2, the isotopic composition of reduced sulfur in
194 trithionate and thiosulfate are isotopically identical.
195
196 The complexity added above in equation 6 allows for numerous products for a given reaction, but still
197 assumes that the fractionation factors involved are static over the time series of the experiment (f_{SO3}) and
198 that there is only one reaction present. If this is true, then the model prediction will match the
199 observation over all values of f_{SO3}. Although we observed a statistically invariant ratio of thiosulfate to
200 trithionate production throughout the reaction (j in Figure 2), suggesting a static set of reactions through
201 the entire experiment, it appears that the net fractionation factor was indeed time-dependent. In the
202 event of an evolving α, the fractionation factor early in the experiment, where the concentration of
203 products remains low, most closely approximates the isotope effect of DsrAB solely reducing sulfite. We
204 explore this time-dependence further in the Appendix for all sampled points on the reaction progress
205 coordinate (f_{SO3}). Thus, for extracting the intrinsic isotope effect associated with enzymatic reduction of
206 sulfite, we focused on data where $f_{SO3} > 0.85$. To do so, we have used our modified Rayleigh-type isotope
207 distillation model in which we account for the production of reduced and oxidized sulfur within aqueous
208 products trithionate and thiosulfate. Procedures for error propagation associated with these calculations
209 are described in the Appendix.
210
211 **Results**
212 We tracked all S pools at each time point. Mass balance was satisfied within ±10% of the initially provided
213 sulfite in every experiment, and within ±5% in 27 of 33 experiments (Figure 2a). The majority of this
214 variance is due to analytical error in the sulfite quantifications. In experiments with the *D. vulgaris*
215 DsrAB, the products were generated with a mean of 19% of the product sulfur forming thiosulfate and
216 the remainder accumulating as trithionate (Figure 2b). This is consistent with previous reports (Drake
217 and Akagi, 1976; 1978), and expected given the absence of active DsrC in these experiments. Some
218 inactive DsrC does accompany the *D. vulgaris* DsrAB during isolation and purification (Oliveira et al.,
219 2008a; 2008b; 2011), however there is no means to recycle this component, and as such, it is not a
220 functional part of the experiment. Therefore, the in vitro sulfite reduction reactions produce thionates
221 rather than sulfide. In our experiments, sulfite was always in excess and never became limiting.
222
223 To extend our studies to a different taxonomic form of the enzyme, we also experimented on the DsrAB
224 from the thermophilic archaeon *A. fulgidus*. This enzyme operates at higher temperature and lacks DsrC
225 in the complex (Schiffer et al., 2008). *A. fulgidus* DsrAB experiments were conducted with 15 mM initial
226 sulfite and at 65°C, where they showed consistent loss of sulfite and accumulation of products between
227 replicates at each time point. Unlike *D. vulgaris* DsrAB experiments, however, only small quantities of
228 product were generated. From these experiments we were able to resolve a complete sample set (i.e.
229 sulfite, sulfonate and reduced S) from one time-point and partial sets from another (i.e. sulfite and
230 sulfonate). Special efforts were made to correct data available on *A. fulgidus* experiments (see the
231 Appendix). The results using DsrAB from *A. fulgidus* are consistent with those of *D. vulgaris*, but with a
232 large calculated uncertainty. We therefore focus our interpretations on the results from the *D. vulgaris*
233 experiments.
234
235 We use the concentrations of sulfite, trithionate, and thiosulfate, as well as the isotopic compositions of
236 each operationally defined product to solve for the fractionations associated with DsrAB. The calculated
237 $^{34}\varepsilon_{DsrAB}$ for sulfite reduction by the *D. vulgaris* DsrAB is 15.3±2.0 ‰ (2σ, Figure 3), where the concurrent
238 fractionation associated with the generation of the sulfonate is -3.2±0.8‰ (2σ). The $^{34}\varepsilon_{DsrAB}$ from *A.*

239 *fulgidus* is generally consistent with the *D. vulgaris* experiments, yielding a reductive fractionation of 16‰
240 (2σ from 22 to 12‰) at 65°C. Large and asymmetric errors on the *A. fulgidus* data are the result of
241 exceptionally small sample sizes, which also precluded the collection of ^{33}S data (see the Appendix).
242 Together, these experiments demonstrate a broad consistency in fractionation by DsrAB over a wide
243 range of temperatures (20 and 30°C for *D. vulgaris*, and 65°C for *A. fulgidis*) and across two Domains of
244 life.
245
246 Fractionation of ^{33}S between sulfite and reduced sulfur by *D. vulgaris* DsrAB is reported as $^{33}\lambda_{DsrAB}$, with a
247 calculated result of 0.5150±0.0012 (2σ) over the initial range of f_{SO3}. The conversion of sulfite to
248 sulfonate yielded a calculated $^{33}\lambda_{DsrAB}$ that changes as the reaction progressed, from 0.495±0.017 (2σ) at
249 $f_{SO3} > 0.85$, towards 0.510 at $f_{SO3} < 0.85$. The experimental error on $^{33}\lambda_{DsrAB}$ is inversely related to the
250 magnitude of $^{33}\varepsilon_{DsrAB}$ (Johnston et al., 2007), thus is larger for sulfonate generation. We interpret the
251 observed fractionation factors between sulfite and reduced S as representing the binding and reduction of
252 sulfite by DsrAB. The fractionation associated with sulfonate production is more difficult to uniquely
253 diagnose given the wide array of potential biotic and abiotic reactions.
254
255 **Discussion**
256
257 Microbial sulfate reduction is a major process in the sulfur cycle and generates characteristic isotopic
258 fractionations. These fractionations are critical in tracing the movement of sulfur within natural settings
259 (marine and lacustrine). Determining the isotope effects associated with key enzymes in this pathway is
260 critical to disentangling biological and physical controls on the distribution of sulfur isotopes among
261 environmental pools of sulfur. In this study we provide the first constraints ($^{34}\varepsilon$ and $^{33}\lambda$) on the isotope
262 effects associated with one such enzyme: dissimilatory sulfite reductase, the central redox enzyme in
263 dissimilatory sulfate reduction. This experimental constraint provides insight and critical boundary
264 conditions for understanding sulfur isotope fractionation by sulfate reducers. Fortunately, half a century
265 of research on sulfur isotope fractionation by MSR in vivo puts in place a series of useful observations
266 that help to guide our interpretation as to the role of DsrAB. This in turn allows significantly greater
267 access to the information locked in sulfur isotope records.
268
269 There is a rich literature of whole cell isotope fractionation data associated with MSR, but information
270 about kinetic isotope effects associated with specific enzymes within the metabolism are entirely lacking.
271 Cellular-level observations include secular and spatial trends in sulfur isotope records attributed to
272 changes in the environmental conditions at the site of MSR, and degree to which biogenic sulfide is
273 preserved in marine sediments (Holland, 1973; Canfield and Farquhar, 2009; Leavitt et al., 2013). The
274 environmental variables most commonly invoked to explain isotopic variability are aqueous sulfate and
275 organic carbon concentrations (Goldhaber and Kaplan, 1975; Habicht et al., 2002; Bradley et al., 2015).
276 Both of these variables ultimately contribute to the net reduction rate and carry independent biological
277 thresholds, one of which ultimately becoming rate-limiting (Bradley et al., 2011; 2015). More
278 specifically, variability in these substrates is manifested as changes in the cell-specific rates of MSR in
279 both the laboratory and natural environment (Goldhaber and Kaplan, 1975; Chambers et al., 1975;
280 Leavitt et al., 2013). In laboratory experiments and natural marine and lacustrine systems, volumetric
281 sulfate reduction rates scale primarily as a function of the availability of sulfate relative to common
282 electron donors like organic carbon (Goldhaber and Kaplan, 1975; Chambers et al., 1975; Leavitt et al.,
283 2013; Sim et al., 2011b). Indeed, sulfate can be non-limiting even in environments with as little as μM
284 sulfate (Nakagawa et al., 2012; Gomes and Hurtgen, 2013; Crowe et al., 2014; Gomes and Hurtgen,
285 2015; Bradley et al.; 2015), assuming organic matter is more limiting to allow a fractionation to occur
286 (Wing and Halevy, 2014; Bradley et al.; 2015). Constrained whole cell (in vivo) laboratory experiments

287 demonstrate that when electron donors are limiting, the magnitude of fractionation between sulfate and
288 sulfide ($^{34}\varepsilon$) carries a nonlinear inverse relationship with cell-specific sulfate reduction rates (Leavitt et al.,
289 2013; Kaplan and Rittenberg, 1964; Chambers et al., 1975; Sim et al., 2011b; Harrison and Thode,
290 1958). Thus, the range of isotopic compositions produced and preserved in natural environments are
291 interpreted as an output of intracellular rates, which scales with enzyme activity associated with microbial
292 sulfate reduction (Leavitt et al., 2013; Goldhaber and Kaplan, 1975).
293
294 In addition to following a rate relationship, fractionation in MSR isotope studies often approaches
295 characteristic upper and lower fractionation limits. Recent experimental work at low sulfate reduction
296 rates captures a $^{34}\varepsilon_{MSR}$ (the net isotope effect of microbial sulfate reduction) of nearly 70‰ (Canfield et
297 al., 2010; Sim et al., 2011a). This magnitude of fractionation approaches the theoretical low temperature
298 equilibrium prediction of 71.3 to 67.7‰ between 20° and 30°C (Farquhar et al., 2003; Tudge and
299 Thode, 1950), inspiring research more directly comparing the biologically catalyzed reversibility of MSR
300 enzymes and that of equilibrium (Wing and Halevy, 2014) (see also (Rees, 1973; Holler et al., 2011;
301 Brunner and Bernasconi, 2005; Farquhar et al., 2003; Bradley et al., 2011; Johnston et al., 2007; Farquhar
302 et al., 2008; Mangalo et al., 2008; Bradley et al., 2015)). These studies are fueled by the knowledge that
303 direct (abiotic) equilibration between sulfate and sulfide at Earth surface temperatures is exceedingly
304 slow, with a half-life of exchange estimated at 1.1×10^{10} (at 30°C) to 1.6×10^{12} years (at 20°C; these values
305 are extrapolated from (Ames and Willard, 1951)). Thus, large fractionations between sulfate and sulfide
306 at Earth surface conditions strongly suggests a role for biology.
307
308 Most experiments with sulfate reducing microorganisms result in isotope fractionations much smaller
309 than would be predicted from abiotic equilibrium estimates. More than half a century of research and 648
310 observations from in vivo MSR experiments capture a median isotope fractionation of 16.1‰ (both
311 $^{34}\varepsilon_{MSR}$ and in sulfite reduction experiments: Figure 4). In fact, half of experimental data fall between 10
312 and 22.5‰. This is consistent with the phenomenology of laboratory experiments being conducted at
313 significantly higher sulfate reduction rates than occur in most natural settings. However, given that all
314 these experiments occurred with the same biochemical network, any enzyme-level explanation for the
315 range of fractionations observed at both high and low sulfate reduction rates must be internally
316 consistent.
317
318 As described above, a suite of enzymes and cofactors drives dissimilatory sulfate reduction. During the
319 reduction of sulfate to sulfide, sulfur isotope effects are likely to result primarily from transformations that
320 involve the making or breaking S related bonds. Initial steps in sulfate reduction, such as transport into
321 the cell and activation via a reaction with ATP to generate APS (Figure 1 (Fritz, 2002)), do not involve
322 the formation of new S linkages, and are not predicted to be associated with primary isotope effects.
323 Influence on the expressed isotopic fractionation due to transport limitation is, however, conceivable.
324 That is, the concentration of sulfate in the cell may influence the expression of downstream isotope
325 effects, altering the net observed $^{34}\varepsilon_{MSR}$. Sulfate transporters may also induce an isotope effect associated
326 with varying membrane fluidity or other strain-specific optima, in response to changing temperature
327 (Kaplan and Rittenberg, 1964; Canfield, 2006), pH (Furusaka, 1961), or as environmental sulfate
328 concentrations become metabolically limiting (Habicht et al., 2005) (see discussion in Bradley et al.
329 2015).
330
331 Primary isotope effects are predicted where bonds are made or broken. APS reductase catalyzes a two-
332 electron exchange that breaks a S-O bond during reduction of APS to generate free sulfite. From the
333 crystal structure of ApsR (Fritz, 2002), it is apparent that the enzyme binds with the APS bound sulfur
334 directly on a nitrogen in the FAD (flavin adenine dinucloetide) cofactor. The product sulfite is then
335 available to interact with DsrAB. This heterodimeric enzyme binds sulfite in an active site containing

336 siroheme. The formation of the Fe-S bond between siroheme and sulfite may be the critical reaction
337 controlling isotope fractionation. Following this, sulfite is proposed to be reduced by the step-wise
338 transfer of two electrons to form S^{2+}, then two additional electrons to form S^0 (Parey et al., 2010). Under
339 in vivo conditions, the S^0 intermediate was suggested to be withdrawn from the DsrAB complex by the
340 small transfer protein DsrC (Oliveira et al., 2008b; Venceslau et al., 2014). Under in vitro conditions,
341 DsrC is generally absent, and the reduced sulfur in the active site may react with excess sulfite, forming
342 thiosulfate and trithionate (Figure 1) (Drake and Akagi, 1976). DsrC is independently regulated in vivo
343 (Karkhoff-Schweizer et al., 1993), and generates the terminal sulfide from DsrAB bound sulfur derived
344 from sulfite (Venceslau et al., 2014). The relative importance of this protein has only been realized in the
345 last few years (Oliveira et al., 2008b; Venceslau et al., 2014), and has an unconstrained isotope effect.

347 In general, the magnitude of the thermodynamically predicted sulfur isotope effect scales positively with
348 the number of bonds are made or broken (Tudge and Thode, 1950; Bigeleisen and Wolfsberg, 1958). As
349 described above, sulfite reduction by DsrAB is a central enzyme in MSR, breaking three S-O bonds
350 (Venceslau et al., 2014; Oliveira et al., 2008b), and therefore knowing the fractionation associated with
351 this step is critical to any predictive MSR isotope model (c.f. (Rees, 1973; Brunner and Bernasconi, 2005;
352 Johnston et al., 2007; Farquhar et al., 2007; 2008; Bradley et al., 2011; Wing and Halevy, 2014; Bradley et
353 al., 2015)). Our direct constraint on the fractionation imposed by sulfite reduction indicates that the
354 published assignments of 25‰ (Harrison and Thode, 1958; Rees, 1973) and 53‰ (Brunner and
355 Bernasconi, 2005) for DsrAB are significant over-estimates. It is perhaps not surprising, given that
356 previous appraisals were generated through various indirect approaches (Harrison and Thode, 1958;
357 Rees, 1973; Farquhar et al., 2003; Johnston et al., 2007; Brunner and Bernasconi, 2005), (Harrison and
358 Thode, 1958; Rees, 1973; Farquhar et al., 2003; Johnston et al., 2007; Brunner and Bernasconi, 2005).
359 As previously highlighted, this represents a major limitation to model applications (Chambers and
360 Trudinger, 1979).

362 Our measured $^{34}\varepsilon_{DsrAB}$ value for sulfite reduction (15.3±2.0‰) is large enough to account for the majority
363 of the fractionations observed in the bulk of published the whole-cell MSR experiments over the last
364 sixty-five years (median of 16.1‰, n = 648; Figure 5). As noted previously, laboratory experiments carry
365 a strong bias toward higher rates of sulfate reduction, and as such, the data compilation should be viewed
366 in this light. As most recently articulated through a series of chemostat experiments (Leavitt et al., 2013;
367 Sim et al., 2011a), the consequence of elevated metabolic rate is a smaller relative $^{34}\varepsilon$. In isotope
368 biogeochemistry, relationships like this often depend on the single slowest overall rate-limiting step
369 within a metabolism (Mariotti et al., 1981; Hayes, 1993). The fractionation limit at high metabolic rates
370 in cultures ($^{34}\varepsilon$ = 17.3±1.3‰), marine sediments ($^{34}\varepsilon$ = 17.3±3.8‰) and DsrAB are statistically
371 indistinguishable (Figure 5). This similarity is consistent with DsrAB as a rate-limiting step explaining
372 the majority of observed fractionation (Figure 5). However, this interpretation omits complexity
373 associated with the metabolic network.

375 This raises an essential question: how does the DsrAB constraint change our understanding of the
376 possible range of fractionations imposed by MSR? For instance, if we assume that DsrAB is the slowest
377 reaction in MSR, then the metabolic steps preceding sulfite ($SO_4^{2-} \Leftrightarrow APS \Leftrightarrow SO_3^{2-}$) will necessarily
378 approach equilibrium (Wing and Halevy, 2014). The thermodynamic predictions would then require an
379 accompanying fractionation approaching 25‰ between sulfate and sulfite at biologically relevant
380 temperatures (the equilibrium fractionation estimate (Farquhar et al., 2003)). At its simplest, this effect
381 would be additive with that of DsrAB (25 + 15.3 ‰, or 40.3‰), which encompasses a majority of
382 experimental MSR isotopic fractionations. However, the lower plateau in fractionation approached at
383 high rates, stemming from the calculations using both modern marine sediment and chemostat data (see

384 the Appendix) – is less than half of this magnitude. That is, the lower plateaus for in vivo fractionation at
385 high rates of 17.3‰ allows only a ~2‰ fractionation partitioned among these upstream steps, if in fact
386 DsrAB is fully expressed. This smaller 'upstream' kinetic fractionation is, however, consistent with the few
387 loose estimates from crude cell extracts and resting cell studies (i.e. not purified enzymes), which
388 putatively suggests a $^{34}\varepsilon$ of 4 to 15‰ for the cumulative activation of sulfate to APS and reduction to
389 sulfite (Ford, 1957; Kemp and Thode, 1968). This may suggest that the sulfate-sulfite conversion (in
390 vivo and in vitro) reflects a predominately kinetic (rather than equilibrium) control. This requires,
391 however, we loosen the degree to which DsrAB is called upon to fully control the net MSR isotopic
392 fractionation, invoking some delicate balance between upstream reactions and that of DsrAB, but
393 maintaining the model where enzyme kinetics (especially DsrAB) will win out over equilibrium effects as
394 sulfate reduction rates move from low to high.
395
396 An alternate explanation is that APS reductase (ApsR) is the rate-limiting step under sulfate replete
397 conditions (Rees, 1973). If this is the case, fractionation imposed by DsrAB is unexpressed, as it is
398 downstream of ApsR (Hayes, 2001; Rees, 1973). If fractionation associated with APS reductase is near
399 17‰, it could alone account for most of the observed fractionation observed at high sulfate reduction
400 rates. The fractionation imposed by ApsR has not been directly measured, though can be proxied from
401 the discussion above. However, evidence against ApsR as the rate-limiting step is shown by studies
402 indicating reversibility of the ApsR (Peck, 1960) and the sulfate reduction pathway (Chambers and
403 Trudinger, 1975; Holler et al., 2011). Recent studies using oxygen isotopes as tracers have demonstrated
404 that some intracellular sulfite is oxidized in vivo back to sulfate (Mangalo et al., 2007; Farquhar et al.,
405 2008; Turchyn et al., 2010; Einsiedl, 2008; Mangalo et al., 2008). These studies demonstrate that sulfite
406 re-oxidation is commonplace in MSR and often quantitatively significant (Antler et al., 2013). This
407 reoxidation is inconsistent with ApsR being rate-limiting under the range conditions tested.
408
409 Any explanation for the net MSR isotopic fractionation must also account for the large fractionations
410 observed at low sulfate reduction rates. These large fractionations are common in nature, and require
411 another type of mechanism. These isotopic fractionations approach but do not reach the theoretical
412 equilibrium values for sulfur isotope exchange between sulfate and sulfide (Figures 4 and 5) (Farquhar et
413 al., 2003; Tudge and Thode, 1950; Johnston et al., 2007). In this context, further analysis to understand
414 intracellular thermodynamics is critical (the redox pairs responsible for various reactions, see (Wing and
415 Halevy, 2014)), along with measurements of the intrinsic isotope effects of other key enzymes in the
416 metabolic network, including ApsR and DsrC. In that sense, this study represents a key first step.
417
418 In parallel to examining the $^{34}\varepsilon$ effects, measuring minor S isotope ($^{33}S/^{32}S$) fractionation provides
419 additional information about the class of reaction mechanism associated with in vitro DsrAB activity. In
420 our experiments, the conversion of sulfite to sulfonate carries a $^{33}\lambda$ of from ~ 0.496 (±0.012, 2σ), evolving
421 toward 0.510 as the reaction proceeds. Sulfite reduction via DsrAB has an invariant $^{33}\lambda$ of 0.5150
422 (±0.0012, 2σ). In cases where $^{33}\lambda$ is 0.515, a purely equilibrium fractionation is often inferred but not
423 required, while values less than this require kinetic effects (Young et al., 2002; Farquhar et al., 2003). In
424 this framework, in vitro sulfonate formation falls under kinetic control, while formation of reduced S
425 could be interpreted as a kinetic or equilibrium reaction. Thus, specific predictions for the DsrAB
426 enzyme require more detailed modeling of the structure and function of the DsrAB enzymatic active site.
427 This level of analysis – where inroads joining empirical work with theory are constructed – is present in
428 analogous systems (Karsh et al., 2012), but absent within the S cycle. Nonetheless, the work here
429 provides the only triple-isotope constraints on enzyme-specific fractionation factors in both MSR and the
430 global biogeochemical S cycle. Further, this approach may prove useful in other enzymatic systems where
431 elements with ≥ 3 stable isotopes are involved (e.g. O, Fe, Ca, Mg, Se, Zn, Mo).
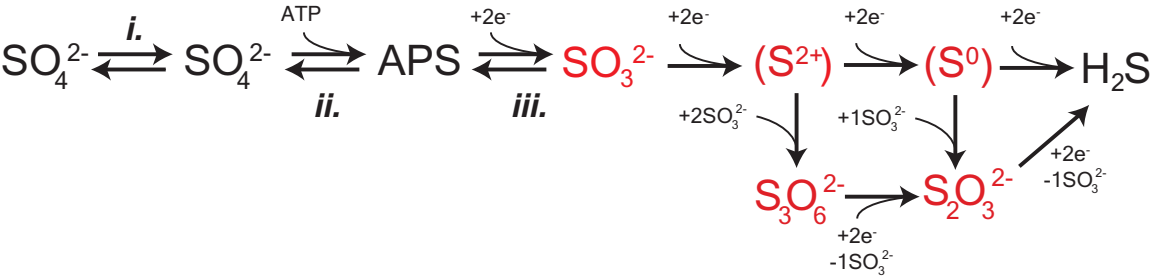
432

Conclusions

Direct constraints on enzymatic isotope effects, when placed in context of laboratory and field observations, represent a key step towards improving our understanding of how environmental factors come to control biochemical sulfur isotope fractionations in nature. Experimental results indicate that the kinetic isotope effect generated by dissimilatory sulfite reductase, the enzymatic core of MSR, generates less than a quarter of the maximum fractionation observed in sulfate reduction experiments and modern marine sediments. However, the $^{34}\varepsilon_{DsrAB}$ aligns nicely with the vast majority of experimental data generated over the last 65 years, as well as chemostat and marine sediment studies sampling high rates of sulfate reduction. The consistency between these published fractionations and the DsrAB isotope effect suggests a fundamental role of this enzyme in setting sulfur isotope compositions. This work highlights the need for further consideration of the allied enzymes in MSR and the likelihood of abiological (and/or equilibrium) effects as microbial sulfate reduction rates slow. Though questions remain, placing quantitative constraints on the core of sulfate reduction – DsrAB – represent a fundamentally new direction in exploring experimental and environmental sulfur isotope records today and throughout Earth history.

Leavitt, Bradley et al. 2015

461   **FIGURES**

462

463

464   **Figure 1.**

465

466

467

Figure 1: A schematic capturing the central role of DsrAB in MSR. The in vivo dissimilatory sulfate reduction pathway, where red highlighted steps represent sulfite reduction by DsrAB in the absence of DsrC, as targeted here in vitro. The constituent steps of MSR relevant to S isotope fractionation are likely APS reduction to sulfite by APSr, sulfite reduction (the subject of this study) by DsrAB, and the terminal production of sulfide by DsrC/DsrMKJOP. The pathway is described in detail in the text.

473

474

11

475 **Figure 2.**
476

477
478
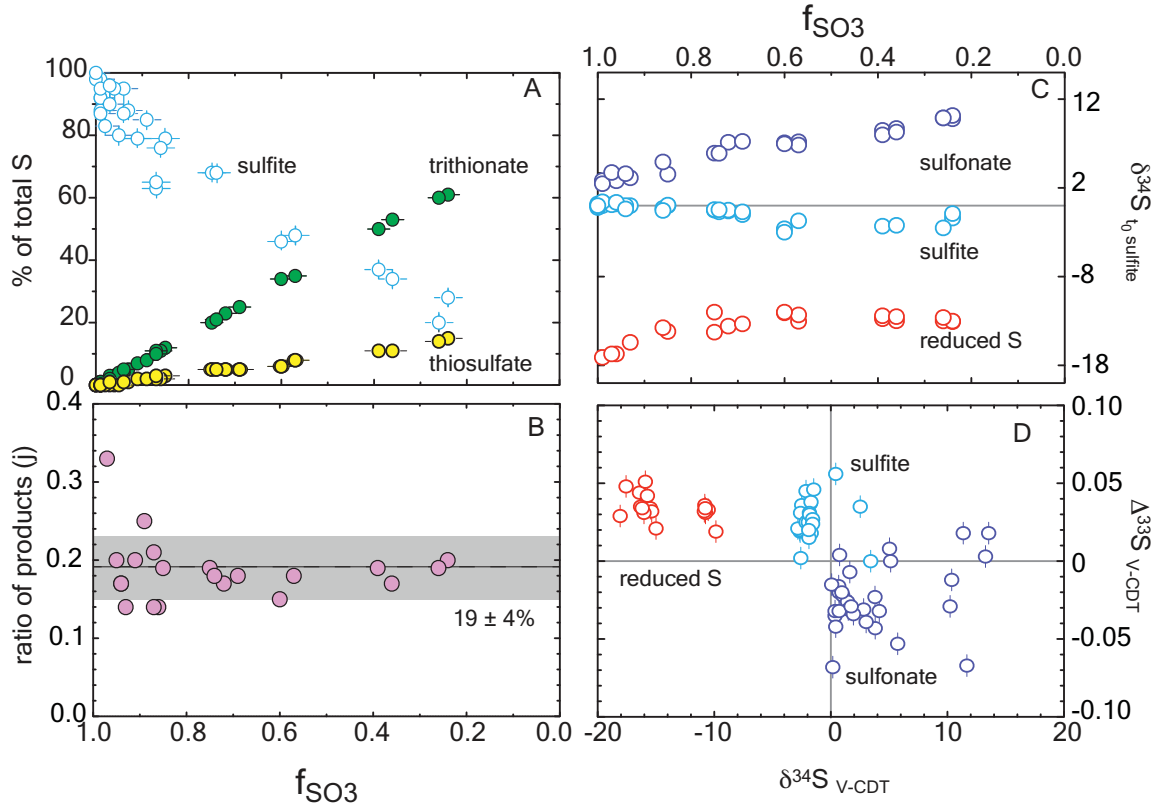
479 **Figure 2: Reaction progress during sulfite reduction with _D. vulgaris_ DsrAB in vitro.** Errors are
480 included in all measurements (2σ) and are smaller than the symbol if not seen. (A) The mol fraction of
481 sulfur in each sulfur product pool as a function of reaction progress, f_{SO3}. Mass balance conservation is
482 discussed in the text. (B) The ratio of products at each time point, demonstrating the constancy of the
483 reaction scheme (denoted as _j_ in the model). This is the ratio of the slopes of the products from A. (C)
484 Major isotope data for each operationally defined sulfur pool as a function of reaction progress, and
485 normalized to the initial sulfite composition. (D) A triple isotope cross plot of the data presented in
486 frame C, normalized to V-CDT.
487

Leavitt, Bradley et al. 2015

488   **Figure 3.**
489
490
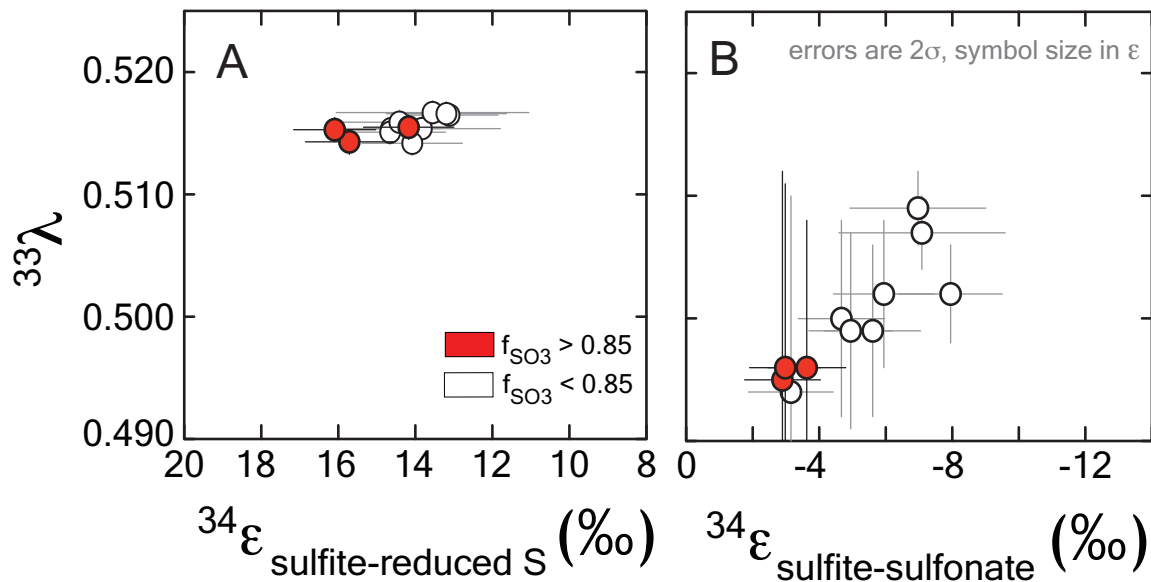
491
492
493   **Figure 3: Sulfur isotope fractionation during sulfite reduction by DsrAB.** Presented here is the
494   fractionation between sulfite and reduced sulfur (within trithionate and thiosulfate) facilitated by in vivo
495   DsrAB (left frame). Initial values of $^{34}\varepsilon_{DsrAB}$ when f_{SO3} is > 0.85 are near 15‰. A small amount of
496   variability accompanies changes in f_{SO3} to < 0.85. Data from *A. fulgidus* overlap *D. vulgaris* DsrAB data
497   (see Figure S2). The minor sulfur isotope fractionation, $^{33}\lambda_{DsrAB}$, is stable near 0.515. Fractionation
498   factors for sulfonate generation, presented in the right frame, are much smaller in $^{34}\varepsilon$ and carry the
499   opposite sign. Both the $^{34}\varepsilon$ and $^{33}\lambda$ evolve over the time course of the experiment, only after f_{SO3} < 0.85.
500   Data and application to calculations are further discussed in the text.
501
502

13

Leavitt, Bradley et al. 2015

503   **Figure 4.**
504
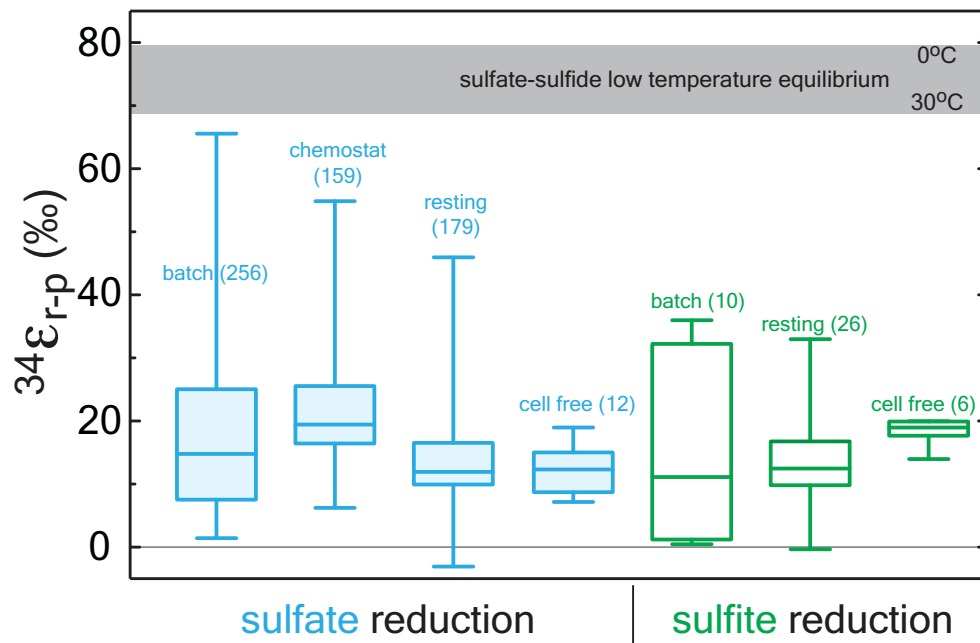
505
506
507   **Figure 4: A box and whisker plot of previously published sulfate (blue) and sulfite (green)**
508   **reduction experiments**. All data is binned by experimental approach. The whiskers reflect the entire
509   range of the data, with the boxes reflecting the middle 50% of the data. The median of the data is
510   represented by the bar dividing the box. The bar running across the top is a temperature dependent
511   prediction based on low temperature thermodynamic equilibrium (Farquhar et al 2003). The statistical
512   method and output are detailed in the Appendix along with the compiled data
513   (http://dx.doi.org/10.6084/m9.figshare.1436115), where all compiled values are from the following
514   sources: (Harrison and Thode, 1957; 1958; Krouse et al., 1968; McCready et al., 1975; McCready, 1975;
515   Sim et al., 2012; 2013; 2011b; 2011a; Johnston et al., 2007; Johnston, 2005; Farquhar et al., 2003; Thode
516   et al., 1951; Bolliger et al., 2001; Knöller et al., 2006; Detmers et al., 2001; Jones and Starkey, 1957;
517   Kleikemper et al., 2004; Mangalo et al., 2008; 2007; Canfield, 2006; Hoek et al., 2006; Pallud et al., 2007;
518   Böttcher et al., 1999; Smock et al., 1998; Kemp and Thode, 1968; Ford, 1957; Leavitt et al., 2013; 2014;
519   Chambers et al., 1975; Davidson et al., 2009; Habicht et al., 2005; Kaplan and Rittenberg, 1964).
520
521

14

522 **Figure 5.**
523

524
525
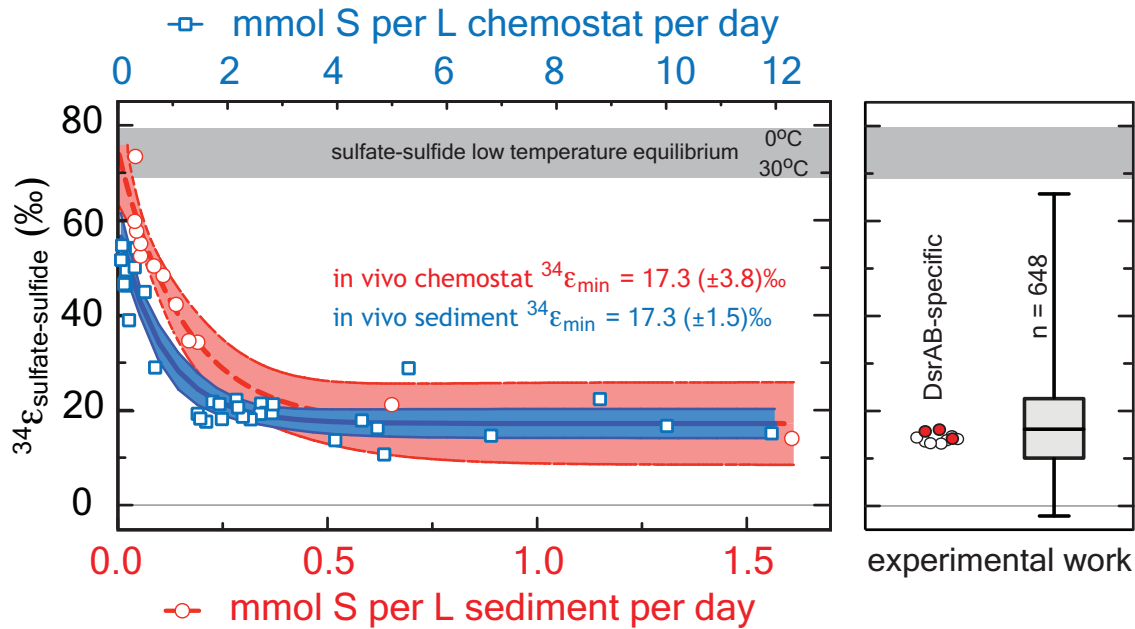
Figure 5: A comparison between modern marine (environmental) and laboratory (experimental) S isotope fractionations, as a function of sulfate reduction rate. These data are further referenced to a statistical distribution of published experimental fractionation data. (A) Fractionation as a function of volumetric sulfate reduction rate from axenic continuous culture experiments (blue squares and regression) (Leavitt et al., 2013) and modern marine sediments (red circles and regression) (Goldhaber and Kaplan, 1975). Solid lines are mean values with shaded regions representing the 95% confidence interval around a non-linear regression. While the upper fractionation limits are offset, perhaps due to differences in biomass per volume of sediment versus volume of chemostat, the limits approached at high reduction rates are statistically indistinguishable at 17.3‰. (B) The fractionation associated with DsrAB experiments, color-coded as in Figure 3 and on the same isotope scale. Also included is a box-whisker treatment of all measured $^{34}\varepsilon$ (n = 648) sulfate and sulfite reduction experiments compiled in Figure 2. Here, the median value is 16.1‰, also statistically indistinguishable from chemostat and modern marine sediments limits at elevated rates of sulfate reduction. Included for reference is the theoretical sulfate-sulfide equilibrium fractionation (gray bar) for 0 to 30°C (Farquhar et al., 2003).

540
541
542
543

15

544   **APPENDIX**

545

546   **Appendix 1:**

547   **Operational definitions of S moieties**

548   In this study we measured the concentrations of three pools: sulfite, trithionate, and thiosulfate;
549   hydrogen sulfide was not detected. We measured the major and minor sulfur isotopic compositions of
550   three operationally defined pools: 'reactant' sulfite (initial and residual), product 'sulfonate', and
551   'reduced product' S. What we refer to as the pooled product 'sulfonate' sulfurs are known in inorganic
552   chemistry as sulfuryl groups (O_2S-X_2), where one of the X's represents an O^-/OH and the other a S in
553   oxidation state 0 (trithionate) or -1 (thiosulfate), meaning the outer sulfuryl-S's are in approximately
554   oxidation state +5 (thiosulfate) or +4 (trithionate), with initial and residual reactant sulfite sulfur in the
555   standard +4. The sulfonate S differs from sulfite S in that it is bound to either an approximately -1 valent
556   sulfur in thiosulfate ($S-S(O)_3^{2-}$) (Vairavamurthy et al., 1993) or as two sulfonates each bound to one
557   sulfur of valence approximately 2+, in trithionate ($(O_3S-S-SO_3)^{2-}$). In this study we refer to the 0 and -1
558   oxidation state sulfurs from trithionate and thiosulfate, respectively, as the 'reduced product' S pool.
559   They are grouped by our operational extraction (see below). For explicit definitions and nomenclature
560   refer to the 'IUPAC Goldbook' (McNaught and Wilkinson, 1997).

561

562   **Appendix 2. Enzyme purification and in vitro experiments**

563   **A2.1 DsrAB isolation and purification**

564   DsrAB was purified from *Desulfovibrio vulgaris* Hildenborough (DSM 644) and *Archaeoglobus*
565   *fulgidus* cells grown in a 30 or 300L batch culture in a modified lactate/sulfate medium (Oliveira et al.,
566   2008a) at iBET (Instituto de Biologia Experimental Tecnológica; www.ibet.pt), grown at 37 or 80°C,
567   respectively. The soluble cell fraction was obtained as previously described (Le Gall et al., 1994; Oliveira
568   et al., 2008a). All purification procedures were performed under atmosphere at 4°C using an AKTA
569   FPLC (Amersham Biotech Pharmacia) with two buffers, (A) 20mM TrisHCl and (B) 50mM TrisHCl
570   with 1M of NaCl (both pH 7.6 and containing 10% glycerol). Buffer (A) was used to equilibrate the
571   columns and buffer (B) to generate the ionic strength gradient. The soluble cell fraction was loaded into
572   a Q-Sepharose fast-flow (XK50/30) column, and a stepwise salt gradient applied, with the DsrAB-
573   containing fraction eluting at 300 mM NaCl. The characteristic DsrAB ('desulfoviridin') absorption peak
574   at 630 nm was used to track the protein, as previously described (Marritt and Hagen, 1996; Wolfe et al.,
575   1994). DsrAB-containing fractions were then loaded into a Q-Sepharose fast-flow (26/10) column and
576   eluted in 250 mM NaCl. To verify enzyme purity, the final DsrAB-containing sample was analyzed by
577   12% SDS-PAGE gel electrophoresis. DsrC is present in the DsrAB preparation from *D. vulgaris*, but
578   remains functionally inactive during in vitro assays as previously described (Oliveira et al., 2008b), and
579   also due to the lack of DsrMKJOP (Venceslau et al., 2014). Thus, we refer only to the 'DsrAB' fraction in
580   the *D. vulgaris* experiments. In the *A. fulgidus* experiments, DsrAB is free of any DsrC. Protein was
581   quantified by the method of Bradford (Bradford, 1976). The *Desulfovirio gigas* [NiFe] hydrogenase used
582   in all assays was purified as described previously (Romão et al., 1997).

583   To ensure the activity of purified DsrAB was not strongly influenced by the high initial
584   concentration of sulfite used in the fractionation experiments (10 or 15mM), we performed small-
585   volume kinetic assays under the same conditions as for isotope measurements. Sulfite alone was
586   measured by HPLC on monobromobimane (MBBr) derivatized samples (Newton et al., 1981). Once
587   the sulfite concentrations for each initial and final (0 and 2 hours) time points were sampled, derivatized,
588   measured and calculated, we applied a non-linear regression formulated from the standard Michaelis-
589   Menten equation, solving for the V_{max} and K_m.

590

591   **A2.2 *D. vulgaris* DsrAB in vitro fractionation experiments in detail**

592   To determine the DsrAB-specific S isotope fractionation factors we designed and executed a
593 series of batch (closed-system) sulfite reduction experiments. The key considerations in experimental
594 design are: (*i*) to provide enough sulfite at t_0 to ensure we generate significant enough quantities of all the
595 product pools so we can measure, at high precision and accuracy, and at multiple [time] points on *f*, the
596 multiple S isotopic composition of each pool (*i.e.*, 2μmols of S per pool per SF_6 measurement on the DI-
597 IRMS, which means 2μmols per fluorination reaction); (*ii*) to provide the proper reaction conditions to
598 allow DsrAB optimal activity for goal *i* (pH = 7.1, T = 20 or 31°C); (*iii*) to ensure hydrogenase activity is
599 not inhibited by the pH chosen (optimum above pH 7.5, activity significantly depleted below pH 6.5, so
600 we chose pH 7.1, to account for optima of both DsrAB and [NiFe]-Hydrogenase); and finally (*iv*) to
601 ensure the sulfite to hydrogen ratio favors sulfite over reductant capacity (i.e., pH_2 in the headspace
602 relative to [sulfite]$_{t0}$), such that no more than 75% of t_0 sulfite is consumed to all products, and less than
603 50% to the reduced S (dictated by the amount of H_2 in the headspace. Finally, (*v*) determining the
604 sampling interval to ensure proper distribution of points along *f*, such that applying a closed system
605 distillation model is possible, and statistically robust. Data plotted in Figure 3 represents experimental
606 results that met all of these conditions. The full experimental results (33 experiments) are contained as a
607 supplemental file (http://dx.doi.org/10.6084/m9.figshare.1436115).

608   All experiments were prepared in an anaerobic chamber. In vitro reactions were carried out in
609 100mL acid-washed, autoclave-sterilized, borosilicate glass bottles sealed with butyl-rubber septa and
610 aluminum crimps. Each bottle contained 50% reaction buffer and 50% gaseous headspace. This was done
611 to sufficient H_2 was present in the headspace to reduce at most 50% of the sulfite, based on an estimate
612 using Henry's law and available solubility constants for H_2 at the given preparation temperatures and
613 headspace pressures. During manipulations in the anaerobic chamber the chamber gas was initially 95:5
614 N_2:H_2. Upon removing the reaction mixture-filled bottles from the chamber, these were capped and
615 crimped, and headspace completely exchanged with deoxygenated 100% Ar, then finally exchanged for
616 100% H_2 to initiate the experiments. Experimental buffer is 50mM phosphate buffer (KP*i*) prepared at
617 pH 6.9±0.05, with final pH is 7.1±0.05 following the addition of the stock Na_2SO_3 solution (the reaction
618 is therefore initiated at 7.1). All reaction solutions contained the following: 50mM KP*i* buffer (final pH
619 7.1±0.05), 10 or 15 mM sodium sulfite, 0.832mM methyl viologen, 242 nM or 315 nM of *D. vulgaris*
620 DsrAB (calculated to give the same activity depending on the DsrAB aliquot selected), and 8.25 nM
621 [NiFe] hydrogenase (297 U/mg). All experimental mixtures and reagents were prepared in previously
622 boiled 18.2MΩ water, cooled under O_2-free N_2.
623

A2.3 *A. fulgidus* DsrAB in vitro fractionation experiments in detail

625   To extend our studies to a different taxonomic form of the enzyme, we used DsrAB from the
626 thermophilic archaeon *A. fulgidus.* This enzyme operates at higher temperature and does not have DsrC
627 present in the complex (Schiffer et al., 2008). The results from these experiments are significantly limited
628 compared to those with *D. vulgaris*, due to too few time points to apply the closed-system model
629 (specifically due to significantly low sample sizes of reduced S for isotope measurements, note the effort
630 made to correct the two data points on *A. fulgidus* reduced-S). Nevertheless, the results obtained are
631 comparable, when considering the measured $\delta^{34}S$. The values for these experiments are presented with *D.*
632 *vulgaris* values in Figure A2.

633   *A. fulgidus* DsrAB experiments were conducted 15mM initial sulfite and 65°C, and showed
634 consistent loss of sulfite and accumulation of products between replicates. We selectively precipitated,
635 separated, and directly measured the ^{32}S-^{33}S-^{34}S-^{36}S compositions from the residual reactant ('sulfite S')
636 and the 'sulfonate S' (($SO_3)_x$). Only the ^{34}S/^{32}S compositions of the 'reduced product S' [$(S)_y$] reservoirs
637 were measured (again, due to significantly small reduced-S samples recovered). From these experiments
638 we were able to get a complete set of samples (i.e. sulfite, sulfonate and reduced S) from one time-point
639 and partial sets from another (i.e. sulfite and sulfonate). We are unable to calculate the $^{34}\varepsilon_{DsrAB}$ for *A.*

640 *fulgidus* directly using our model of sulfite reduction experiments due to the dearth of time points (points
641 on *f*). However, the *A. fulgidus* isotope values agree with those measured sulfite, sulfonate and reduced S
642 moieties for *D. vulgaris* (Figure A2). This general agreement between *D. vulgaris* and *A. fulgidus* DsrAB,
643 independent of temperature or phylogenetic origin is perhaps unsurprising, given that previous
644 theoretical predictions deemphasize the role of temperature in determining the magnitude of *kinetic*
645 isotope effects (Bigeleisen and Wolfsberg, 1958). Furthermore, these enzymes tightly share active site
646 structures (Oliveira et al., 2008b; Parey et al., 2013).
647
648 **Appendix 3. Analytical methods & data handling**
649 **A3.1 Quantification of dissolved species**
650   To quantify sulfite and bisulfite concentration in solution we adapted a protocol to quantify SO_2
651 dissolved in water (Grant, 1947), referred to as the 'Fuschin' assay from here foreword. Our protocol is
652 specific to the in vitro DsrAB assay conditions. It was determined that matrix matching between samples
653 and standards and the exclusion of oxygen is critical to a successful and reliable assay. Furthermore, we
654 determined trithionate, thiosulfate, sulfate, and zinc sulfide solids do not interact with this color-reagent
655 in the assay. The Fuschin assay is useful over a range of 0-40 nanomoles of sulfite in the final assay
656 volume of 1mL. Standards of sodium sulfite (Na_2SO_3 anhydrous, analytical grade) were prepared
657 immediately before the assay is performed in deoxygenated water (boiled and degassed with N_2) or KP*i*
658 buffer. The reaction mixture is composed of 0.04% w/v Pararosaniline HCl (analytical grade) in 10%
659 H_2SO_4 (analytical grade) v/v, prepared stored in an aluminum-foil wrapped tube or amber-glass bottle at
660 4°C; and 3.7% formaldehyde (HCHO) prepared fresh each day by diluting 37% (stock) formaldehyde
661 1:10 water. The reaction is performed on the bench working under N_2 flow, or in an anaerobic chamber.
662 A detailed step-by-step protocol is available in (Leavitt, 2014).
663   Trithonate and thiosulfate were measured by a modified cyanolysis protocol (Kelly and Wood,
664 1994; Kelly et al., 1969; Sörbo, 1957). We primarily employed the method of Kelly and Wood (Kelly and
665 Wood, 1994) modified in the following manner: the reaction volumes were reduced to 10 rather than 25
666 mL's (still in volumetric flasks) and we used nitric rather than perchloric acid. Nitric acid was used in the
667 original version of this method (Sörbo, 1957), allowing us to avoid the significant hazards of working
668 with significant volumes of perchloric acid. Samples were added to the reaction buffer to fit within the
669 range of ferric thiocyanate standards (prepared from potassium thiocyanate as a simple standard and
670 thiosulfate as a reaction standard) from 5 to 25 μM (final concentration in the 10mL reaction), as well as
671 'blanks' prepared from the in vitro assay reaction buffer (50 mM potassium phosphate buffer at pH 7).
672 This is typically 400 μL of in vitro solution added to the 10 mL cyanolysis reaction, in duplicate per
673 method (2X thiosulfate determinations and 2X trithionate determinations). A detailed step-by-step
674 protocol is available in (Leavitt, 2014).
675   For sulfide quantifications, we preserved samples in zinc acetate (2% w/v) from each closed
676 system reaction, using a modified Cline (Cline, 1969) method. Analytical grade sodium sulfide (>98.9%
677 Na_2S*9H_2O) was used as the standard, and prepared in deoxygenated (boiled and N_2-sparged) in vitro
678 reaction buffer, by precipitating the sulfide with excess zinc acetate (anhydrous), mimicking our sampling
679 protocol. A detailed step-by-step protocol is available in (Leavitt, 2014). In all samples no sulfide was
680 detected above the determined detection limit of 6.25 μM. From the literature reports where membrane
681 fractions were omitted (Drake and Akagi, 1978), signifying a lack of DsrC re-cycling mechanism
682 (Oliveira et al., 2008b; Bradley et al., 2011), we expected little to no sulfide. This is further supported by
683 the closure of S mass balance at each time-point from each experiment, within analytical error (see main
684 text). Blanks were prepared identically to those in the cyanolysis protocol.
685
686 **A3.2 Sample preparation for S isotope analysis**
687 All S-bearing samples for S-isotope analyses (ultimately as SF_6 and/or SO_2) were removed from the in
688 vitro reaction solution (50mM potassium phosphate) following a sequential precipitation protocol,

689 inspired by that of Smock and colleagues (Smock et al., 1998). Our protocol reflects our specific
690 experimental setup and the pools we aimed to isolate and purify: sulfite (and any trace sulfate), sulfonate,
691 and reduced product S. Samples of the residual reactant (sulfite) and pooled products (reduced product
692 S and sulfonate S) were removed from the in vitro reaction mixture by sequential precipitation and
693 filtration or centrifugation to isolate solid-phases $Ag_2S_{(s)}$ (reduced product), $BaSO_{3(s)}$ (sulfite), $BaSO_{4(s)}$
694 (sulfonate) by the extraction scheme modified from our recent work (Leavitt et al., 2014) and detailed
695 elsewhere (Leavitt, 2014). Samples were captured as $BaSO_{3(s)}$, $BaSO_{4(s)}$ or $Ag_2S_{(s)}$, respectively. Sub-
696 samples of the reduced product Ag_2S were directly fluorinated (after the below washing steps were
697 carried out to ensure clean Ag_2S), or in the case of the sulfonate S-pool, collected from the AVS residue
698 and converted from $BaSO_4$ to Ag_2S by the method of Thode (Thode et al., 1961), according to the
699 protocol we recently published (Leavitt et al., 2013). Novel to this study: all sulfite samples (reacted as
700 $BaSO_{3(s)}$) were oxidized with peroxide prior to 'Thode'-reduction (detailed protocols for these methods
701 are available in (Leavitt, 2014)). All samples entering the elemental analyzer isotope ratio mass
702 spectrometer (EA-IRMS), and combusted to and analyzed as SO_2, are prepared as dry $BaSO_{3(s)}$, $BaSO_{4(s)}$
703 or $Ag_2S_{(s)}$. All samples for quadruple S isotope analysis enter the fluorination line as pure dry $Ag_2S_{(s)}$.
704
705 **A3.3 Major S-isotope ($^{34}S/^{32}S$) ratios measurements**
706 $\underline{C}$ontinuous $\underline{f}$low $\underline{i}$sotope $\underline{r}$atio $\underline{m}$ass spectrometric (CF-IRMS) measurements of the three S-
707 bearing pools of interest, sulfite, sulfonate and reduced product S, were performed as follows: 0.4mg
708 (±0.05mg) $BaSO_3$, $BaSO_4$ or Ag_2S were converted to SO_2 by combustion at 1040°C in the presence of
709 excess V_2O_5 (Elemental Analyzer, Costech ECS 4010) and analyzed by continuous flow isotope ratio
710 mass spectrometry (SD = ±0.3‰; Thermo-Finnegan DELTA V Plus). All samples yielded clean
711 chromatography and most m/z 66 amplitudes (corresponding primarily to the $(^{16}O^{34}S^{16}O)^+$ ionization
712 product) within the range of in-run standards (IAEA: S1, S2, and S3 for Ag_2S or SO5, SO6, and NBS-127
713 for $BaSO_4$ and $BaSO_3$). Some sulfite precipitates ($BaSO_{3\_sulfite}$), though not any of the sulfate or sulfide
714 precipitates ($BaSO_{4\_sulfonate}$ or $Ag_2S_{\_reduced\ product}$) produced atypical weight to m/z 66 response to what we
715 regularly note with lab standards of $BaSO_3$ or $BaSO_4$ – specifically the signal was less than predicted,
716 likely due to occlusion of phosphates (from the in vitro reaction buffer) in the barium sulfite matrix. As a
717 result, we use the m/z 66 to $BaSO_3$ weight ratio (mg of $BaSO_3$ per unit area of the m/z 66 peak) to
718 calculate the desired sample weight to achieve standard signal size, re-weighed and re-
719 combusted/measured the requisite samples, and in all cases achieved m/z 66 peak areas in the range of
720 our IAEA $BaSO_4$ and in-house $BaSO_3$ standards. Each standard is measured at least 4x in-run and each
721 sample 2-3x (when sufficient sample is available). This simplifies the scale-conversion calculation for
722 taking samples referenced in-run to in-house standard tank gas ($HAR1_{SO2}$) and ultimately to the
723 international reference frame (V-CDT).
724
725 **A3.4 Multiple S-isotope ($^{33}S/^{32}S$, $^{34}S/^{32}S$, $^{36}S/^{32}S$) ratio measurements**
726 Duel-inlet (DI-IRMS) measurements of all four stable S isotopes (^{32}S, ^{33}S, ^{34}S, ^{36}S) from the
727 three S-bearing pools of interest, sulfite, sulfonate and reduced product S, were performed as previously
728 described (Leavitt et al., 2013; 2014). Briefly, all samples for quadruple S-isotope analysis, prepared dry
729 and clean Ag_2S (described above), were fluorinated under 10X excess F_2 to produce SF_6, which is then
730 purified cryogenically (distilled at -107°C) and chromatographically (on a 6' molecular sieve 5Å inline
731 with a 6' HayeSepQ 1/8"-stainless steel column, detected by TCD). Purified SF_6 was measured as SF_5^+
732 (m/z of 127, 128, 129, and 131) on a Thermo-Finnegan Scientific MAT 253 (SD: $\delta^{34}S$ ±0.2, $\Delta^{33}S$
733 ±0.006‰, $\Delta^{36}S$ ±0.15‰). All isotope ratios are reported in parts per thousand (‰) as experimentally
734 paired sulfates and sulfides measured. Long-term running averages and standard deviations are calculated
735 from measures of IAEA standards: S1, S2, S3 for sulfides or NBS-127, SO5, SO6 for sulfates. Isotope
736 calculations and notation are detailed in the text. Standard deviations for each value is estimated as
737 reported previously (Johnston et al., 2007) with previous inaccuracies in the transcription corrected here.

738

A3.5 Scale-compression correction calculations for small S samples

739

740   Experiments with *A. fulgidus* yielded small amounts of product (0.35 to 0.01 mg), which
741 required additional data handling during isotope analysis. Given the small size of these samples, we ran
742 each sample only once and bracketed the samples (n = 2) with a series of standards: IAEA S1, S2 and S3
743 (n = 16, 14, and 14, respectively) run over a size series that captured the sample sizes, all by CF-IRMS
744 only. As expected, we observed that the measured isotopic composition of the standards varied non-
745 linearly as a function of signal intensity (monitored as peak integrated areas and peak intensities on m/z
746 64 and 66 for SO_2^+ and 48 and 50 for SO^+). The size dependence on the isotopic composition (handled
747 as ^{50}R and ^{66}R, which are the 50/48 and 66/64, respectively) scale compression is calculated as a

748 proportional change. For SO (*correction factor* in Figure A3) it scales as: $\left| \frac{^{50}R_{predicted} - {}^{50}R_{measured}}{^{50}R_{predicted}} \right|$. We

749 focus on SO here as these samples yielded sharper chromatography on slightly different sized signals
750 (due to resistor differences between SO and SO_2 cups – 3 x 10^{10} Ω and 1 x 10^{10} Ω respectively). Thus,
751 using the three IAEA standards, we developed a correction whereby we solve (in the standards) for the
752 non-linear features of the data as it relates to signal intensity (here monitored as the peak integrated area
753 on mass 48 – ^{32}SO). This is shown in Figure A3. After this correction is applied to $^{50}R_{measured}$, SO data is
754 converted to an SO_2 scale (see Figure A3), which is a linear transfer function again derived from IAEA
755 standard data. The final correction places all the data (now on a SO_2 scale against in-house reference SO_2
756 tank gas) to the V-CDT scale. To review, we perform the following steps 1) correcting the ^{50}R on SO for
757 sample size, 2) convert ^{50}R to ^{64}R (against tank gas), and finally 3) convert all data to a VCDT scale.

758   The largest source of error in this treatment is associated with the sample size correction. As
759 such, we propagate the error associated with the fit in Figure A3 to determine the uncertainty in the final
760 isotope value. As expected, for small samples this error is quite large (Figure A2), with the value
761 decreasing in absolute magnitude as signal intensity (peak integrated area) increases. We also compare
762 these error estimates to the calculated shot noise for this measurement (pink line in Figure A3d). As is
763 presented below, our regressed error is in excess of the shot noise limit. Similarly, the error on the
764 population of standards that were used in deriving this fit is ~1‰ (n = 44).

765

766 **Appendix 4.**

767 **4.1   The closed-system distillation model for a more complex network**

768   There exists the possible mixing of multiple fractionation factors later in the experiment (f <
769 0.85). The approach outlined in the main text yielded results in which the observed fractionation factor
770 between sulfite and reduced pools appeared to change as a function of *f*, when f < 0.85 – that is, later in
771 the reaction, when back-reactions are more likely (Figure A4). One explanation for this apparent
772 behavior is that the reduced pool is not the product of a single set of reactions but of multiple reactions.
773 The most plausible explanation for this is that some fraction of the reduced pool is derived from the
774 sulfonate pool rather than being derived solely from sulfite, particularly later in the in vitro experiment
775 (*i.e.* at values of *f* < 0.85). Previous work (Parey et al., 2010; Drake and Akagi, 1978; 1977) has
776 demonstrated that DsrAB is capable of reducing trithionate to thiosulfate, and thiosulfate to sulfite and
777 sulfide, which was confirmed with the *D. vulgaris* enzyme.

778   We can constrain the magnitudes of the fractionation factor related to the conversion of the
779 sulfonate to reduced S through the following steps. First, utilizing the framework given above to solve for
780 α_{red} for the time points where *f* is nearest to 1. As these measurements are obtained at the lowest
781 concentrations of product, we assume that this result gives an estimate for α_{red} that reflects the production
782 of reduced S from sulfite only, with minimal input of reduced S derived from sulfonate. Second, we write
783 an equation for R_{red} as a function of α_{red}, R_{SO3}, and R_{ox}:

784

785 Equation A1. $R_{red} = X_{SO3}\alpha_{red}R_{SO3} + (1 - X_{SO3})\alpha_{unk}R_{ox}$,

786

787 where X_{SO3} is the fraction of R_{red} generated directly from sulfite and α_{unk} is the unknown fractionation
788 factor between R_{ox} and R_{red}. This equation is then rewritten and solved for α_{unk} as a function of the other
789 parameters over a range of values of X_{SO3} (0.01 – 0.99). This does not yield a unique solution for the
790 unknown fractionation, but constrains its value given the relative importance of the contribution to the
791 reduced sulfur pool of both sulfonate and sulfite. We assume that the *relative* contribution of the
792 secondary reaction is invariant over the course of the reaction, thereby manifesting as no change in *j*.
793

794 **A4.2 Error propagation calculation for the closed system model estimates**
795   The error associated with calculations of $^{33}\lambda$ (approximately the slope of a $\delta^{33}S$ vs. $\delta^{34}S$ line) is
796 highly sensitive to the length of the line (total ^{34}S range, $^{34}\varepsilon$) and modestly related to the residual around a
797 mass-dependent theoretical prediction (the standard deviation on $\Delta^{33}S$ is often used here (Johnston et
798 al., 2007; Farquhar et al., 2003). To approximate the standard deviation (σ) associated with our $^{33}\lambda$
799 calculation, we propagate our measurement errors ($\delta^{34}S$, concentration, etc.). We keep with the
800 presumption that mass-dependence will dictate the $\delta^{33}S$, once the new $\delta^{34}S$ is calculated. This stems from
801 the fact that the error in $\delta^{34}S$ and $\delta^{33}S$ are highly correlated, meaning that the error in $\Delta^{33}S$ is significantly
802 smaller (~0.008‰) than that for $\delta^{33}S$ (~ 0.1‰). As our fractionation factor model is based on a closed-
803 system distillation equation (see above), we perform an error propagation on an equation of the form: R_f
804 $= (R_0)\,(f^{(\alpha-1)})$, where we are most interested in accounting for the analytical errors on the isotope
805 measurement (σ_R, 0.2‰/1000) and the uncertainty on *f*. The second term is critical here as we are
806 independently determining *f* from concentration measurements in the experiment, with a standard
807 deviation on sulfite concentration measurements of 3%. We use this value moving forward as a metric of
808 σ_f. To simplify the presentation, we let X = (α -1) and Z = f^X. Following typical error propagation for
809 power law and multiplicative relations (Bevington and Robinson (2003) page 43-46) (Bevington and
810 Robinson, 2003), we find:

811 Equation A2. $$\frac{\sigma_Z}{Z} = \sqrt{\left(\frac{X\sigma_f}{f}\right)^2}$$

812 which then can substitute into the final form of:

813 Equation A3. $$\frac{\sigma_{R_f}}{R_f} = \sqrt{\left(\frac{\sigma_Z}{Z}\right)^2 + \left(\frac{\sigma_{R_0}}{R_0}\right)^2}$$

814 The σ_{Rf} is then converted into ‰ units (through multiplying by 1000) so that it can be inserted into the
815 updated (Johnston et al., 2007) error equation for $^{33}\lambda$, presented here:

816 Equation A4. $$\sigma_\lambda = \sqrt{\sigma^2_{\Delta^{33}S} * \left(\frac{\partial\lambda}{\partial\Delta^{33}S}\right)^2 + \sigma^2_{\delta^{34}S} * \left(\frac{\partial\lambda}{\partial\delta^{34}S}\right)^2}$$

817   ,

which can be broken down into:

818 Equation A5. $$\frac{\partial\lambda}{\partial\Delta^{33}S} = \left\{ \frac{1}{\ln\left(\frac{\delta^{34}S}{1000}+1\right)} * \frac{1}{\left(\frac{\Delta^{33}S}{1000}+\left(\frac{\delta^{34}S}{1000}+1\right)^{\lambda_{RFL}}\right)} * \frac{1}{1000} \right\}$$

819

and

Leavitt, Bradley et al. 2015

820

821 Equation A6.

$$\frac{\partial \lambda}{\partial \delta^{34}S} = \left\{ \frac{1}{\ln\left(\frac{\delta^{34}S}{1000}+1\right)} * \frac{1}{\left(\frac{\Delta^{33}S}{1000}+\left(\frac{\delta^{34}S}{1000}+1\right)^{\lambda_{RFL}}\right)} * \lambda_{RFL}\left(\frac{\delta^{34}S}{1000}+1\right)^{\lambda_{RFL}-1} * \frac{1}{1000} \right\} +$$

$$\left\{ \ln\left(\frac{\Delta^{33}S}{1000}+\left(\frac{\delta^{34}S}{1000}+1\right)^{\lambda_{RFL}}\right) * \frac{-1}{\left(\ln\left[\frac{\delta^{34}S}{1000}+1\right]\right)^2} * \frac{1}{\frac{\delta^{34}S}{1000}+1} * \frac{1}{1000} \right\}.$$

822

823 As noted above, the error on lambda σ_λ is dependent on the $\delta^{34}S$ and $\Delta^{33}S$. The subscript *RFL* represents
824 the reference fractionation line, which for $^{33}\lambda$ is 0.515, and for $^{36}\lambda$ is 1.90. Data for $\delta^{36}S$ are not discussed
825 in the text, as they yield the same conclusions as $\delta^{33}S$, but are included here in Dataframe S1
826 (https://github.com/bradleylab/DsrAB_enzyme_models).
827   In total, this leaves our error estimate a function of the following five variables: $^{34}\varepsilon$, σ_R, f, σ_f, and α.
828 The final error is not an evenly weighted sum of these variables, and in the case presented here, most
829 heavily influenced by the error in concentration data (σ_f). A sensitivity analysis (Figure A6) on this
830 exercise demonstrates that the errors in f far outweigh the analytical uncertainty in a measurement of R,
831 and dominate the magnitude of the final σ_{Rf}.

832
833

834 **Appendix 5. Data compilations and statistical analysis.**

835 **A5.1   Compilation and statistical analysis of pure-culture MSR fractions**
836   To place our DsrAB enzyme-specific fractionation factor in context with the previous 65 years of
837 pure-culture experimental work, we compile all available observations from studies using axenic cultures
838 of MSR (Figure 4), in the following experimental systems: *batch* (closed-system, in vivo, whole-cell),
839 *chemostat* (open-system, in vivo, whole-cell), *resting* (closed-system, in vivo, whole-cell, not growing),
840 *cell-free* (closed-system, ex vivo crude cell extracts, not growing). From these four types of experiments
841 we further subdivide experiments into where sulfate was reduced to sulfide or sulfite was reduced to
842 sulfide. We count each experimental determination ($^{34}\varepsilon_{r-p}$) and compile them all in the supplemental data
843 files (http://dx.doi.org/10.6084/m9.figshare.1436115), from experiments where less than 10% of the
844 reactant S-species was consumed. Herein we calculate and present column statistics (box-whisker plots
845 in Figure 4) using *Prism5c* (GraphPad, San Diego, CA). The key finding here is that the majority of the
846 means from each set of experiments is significantly less than the previous estimates for the fractionation
847 factor associated with DsrAB (25 to 53‰ (Harrison and Thode, 1957; Rees, 1973; Brunner and
848 Bernasconi, 2005; Farquhar et al., 2003; Johnston et al., 2007)), and that the mean values from all 650+
849 experimental determinations, regardless of experiment type or whether it was a sulfate-sulfide or sulfite-
850 sulfide experiments, the grand mean for $^{34}\varepsilon_{r-p}$ falls at 17.9‰ (median at 16.1‰), with the 25th and 75th
851 percentile's falling at 10‰ and 22.5‰, respectively (Figure 5) – these are all well within the maximum
852 fractionation accounted for by the sum of our DsrAB value (15.3‰) and our literature derived range for
853 sulfate reduction to sulfite (~4 to 15‰), for a total of 19.3 to 30.3‰ (*see* main text).
854

855 **A5.2   Literature estimates of fractionation during sulfate activation to sulfite**
856 The upstream kinetic isotope fractionation, the result of enzyme mediated sulfate/sulfite exchange in
857 cell-free extract experiments, is between 4 and 15 ‰ (compilation files:
858 http://dx.doi.org/10.6084/m9.figshare.1436115). The mean of these experiments is $^{34}\varepsilon_{SO4/SO3}$ = 9.5‰,
859 $CI_{95\%}$ = 7.2 to 11.9‰, with and n = 12 (column statistics are also permanently available at:
860 http://dx.doi.org/10.6084/m9.figshare.1436115) (Harrison and Thode, 1958; Kaplan and Rittenberg,
861 1964; Kemp and Thode, 1968; Ford, 1957). Deconvolving this aggregated fractionation factor
862 ($^{34}\varepsilon_{SO4/SO3}$) in vitro is a target for future pure enzyme experiments focusing on the constituent steps
863 (enzyme specific $^{34}\varepsilon$), as well as the minor isotope fractionations associate with each (*i.e.* $^{33}\lambda$'s).
864 These values represent the fractionation across the sum of the steps incorporating sulfate
865 activation to APS and its concomitant reduction to sulfite (Figure 1). It is important to note that these
866 values were determined using crude-cell extracts, rather than purified enzymes, and not measured over a
867 range of reaction progress (as in Figure 2). Further, available data do not allow for the evaluation of mass
868 balance closure, as we have done here for DsrAB. Given our present understanding of the enzymes
869 involved in this process (Bradley et al., 2011; Pereira et al., 2011), sulfate transport into the cytoplasm
870 followed by activation to APS (Sat) are not likely to directly impact S-isotope compositions, whereas the
871 reduction of APS (APSr) most likely does, due to the breaking of a S-O bond. The sum of transport, Sat
872 and APSr fractionations sit immediately upstream of the DsrAB. Both of these constraints ($^{34}\varepsilon_{SO4/SO3}$ and
873 $^{34}\varepsilon_{DsrAB}$) are interpreted in the context of the MSR data compiled from the literature, which includes lab
874 experiments, natural waters and sediments, as discussed in the main text (Figure 5).
875
876 **A5.3   Statistical analysis of laboratory chemostat and marine sediment fractionations**
877 To apply the compiled sedimentary sulfate reduction rates from Goldhaber & Kaplan
878 (Goldhaber and Kaplan, 1975), we re-plot their log-scale values to a linear scaling (Figure 5) and apply
879 the same non-linear regression one-phase decay model ($Y = (Y_0 - \text{Plateau})e^{(-KX)} + \text{Plateau}$) from
880 our recent work on fractionation—rate relationships in MSR (Leavitt et al., 2013), minimizing variance
881 to arrive at the following parameters: Y_0 = 73‰, plateau = 17.3‰, and a decay-constant (K) of 6.4
882 (Figure 5). For the chemostat (open-system) MSR data in the study where we derived this regression
883 model (Leavitt et al., 2013), we re-scale the cell-specific MSR rates to basic volumetric fluxes by
884 multiplying out the number of cells at each sampling point, using the chemostat values from our recent
885 study (Leavitt et al., 2013). Applying the same one-phase decay model and minimize variance, we
886 calculate the following parameters: Y_0 = 56.5‰, plateau = 17.3‰, and a decay-constant (K) of 0.054. All
887 regressions were calculated using *Prism5c* (GraphPad, San Diego, CA).
888
889
890

891 **APPENDIX FIGURES**

892

893 **Figure A1.**

894

895
896
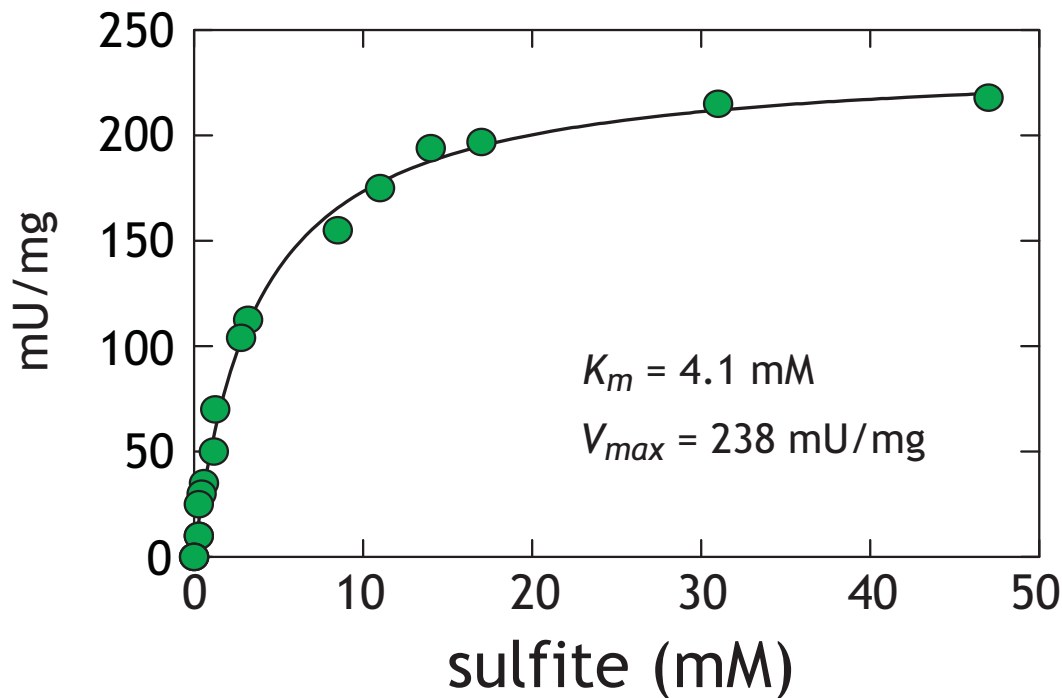
897 **Figure A1.** Activity assays with *D. vulgaris* DsrAB. The difference between initial and final concentration
898 of sulfite after two hours was used to calculate the rate. The Michaelis-Menten equation $\left(\mathbf{Y} = \frac{\mathbf{V_{max} \times X}}{\mathbf{K_M + X}}\right)$
899 was solved for experimental K_m and V_{max} under our conditions. The analytical error is less than the size of
900 the symbols ($2\sigma = 1\mu M$). One unit (U) is defined as the quantity of enzyme that catalyzes the conversion
901 of one micromol of substrate per minute. At both 10 and 15mM initial sulfite we are assured to be well
902 above the apparent DsrAB K_m for sulfite. Reaction inhibition was not observed at sulfite concentrations
903 as high as 50 mM (Soriano and Cowan, 1995; Wolfe et al., 1994).

904

905 **Figure A2.**
906
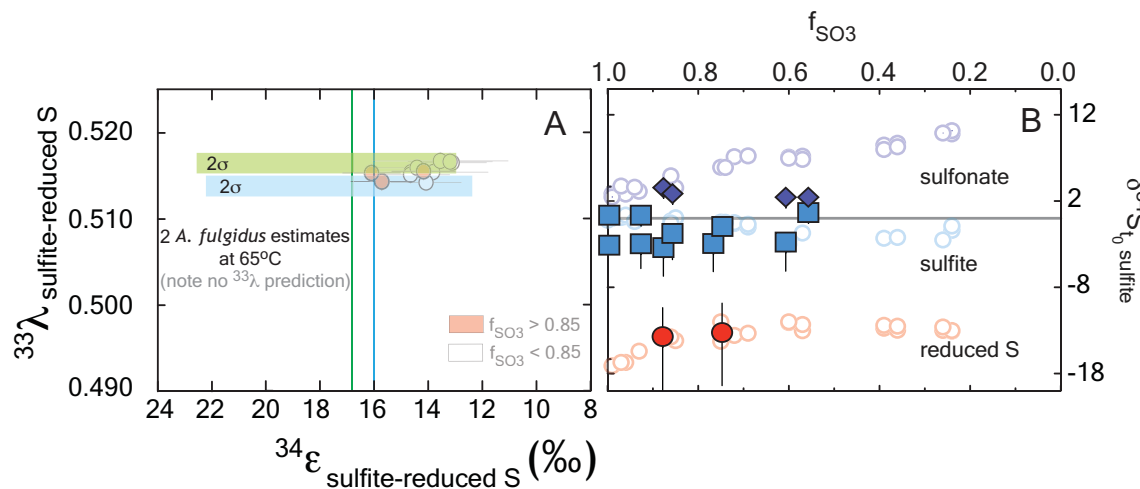
907
908
909 **Figure A2.** The major isotope ratios (δ^{34}S) reported relative to the composition of sulfite at t_0, for the *A.*
910 *fulgidus* (closed symbols) and *D. vulgaris* (open symbols) experiments both as a function of reaction
911 progress. The samples sets show a general consistency, particularly at the reduced S sites, despite the
912 significant offet in temperature (20-30°C for *D. vugaris* relative to 65°C for *A. fulgidus*), consistent with
913 kinetic theory (Bigeleisen and Wolfsberg, 1958), where temperature should impart a minimal effect over
914 this range. The asymmetric error bars on reduced S moieties are a function of the non-linear correction
915 for small sample sizes available for isotope ratio measurements (*see* Appendix text for details).
916
917

918

Leavitt, Bradley et al. 2015

919   **Figure A3.**

920
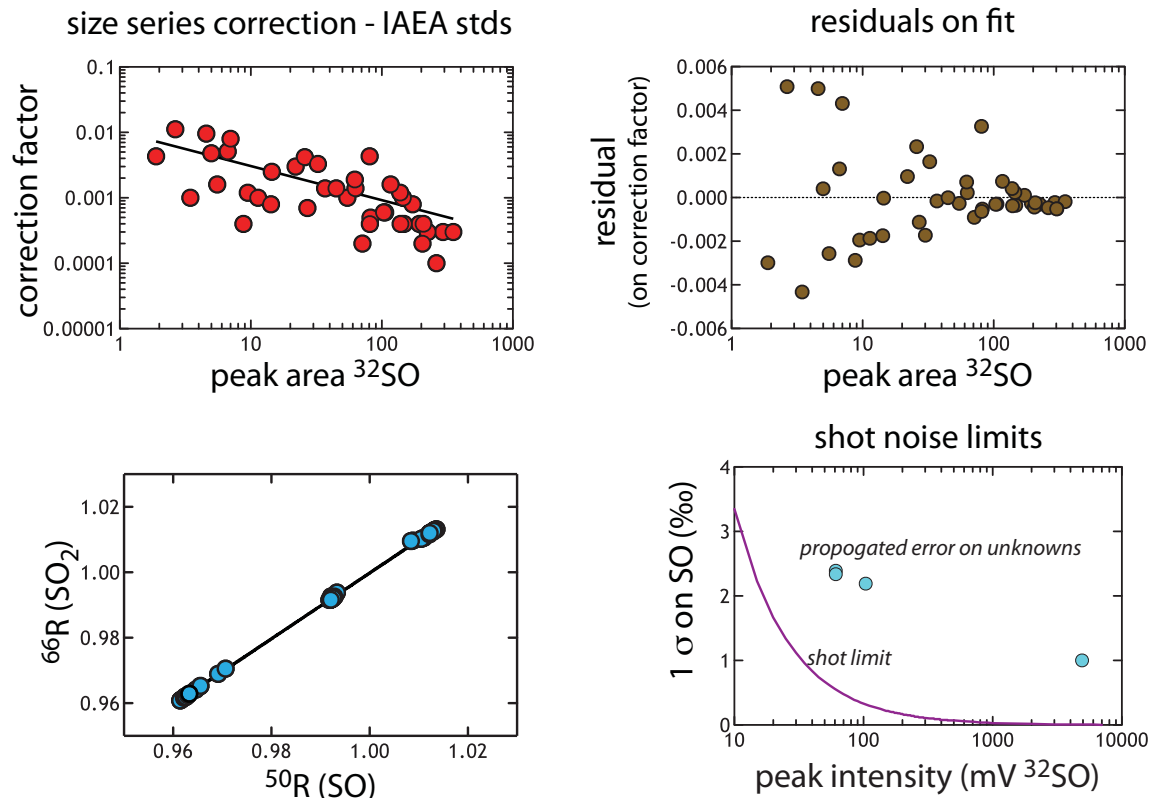
921
922   **Figure A3.** The size series correction calculated from IAEA standards (n = 44). (A) Plots the correction

923   (value from $\left| \dfrac{{}^{50}R_{predicted} - {}^{50}R_{measured}}{{}^{50}R_{predicted}} \right|$ against peak-integrated area). (A) Shows the calculated residual

924   around that fit, demonstrating a symmetric distribution that scales with peak area. This is an illustration
925   of the goodness of the fit. (C) The regression used to convert SO data to an SO_2 scale. (D) The
926   calculated shot noise for SO as a function of signal intensity (peak height in mV). This precision limit is
927   below that which we propagate through the correction, and is provided for reference here.

928

929   **Figure A4.**

930

931
932
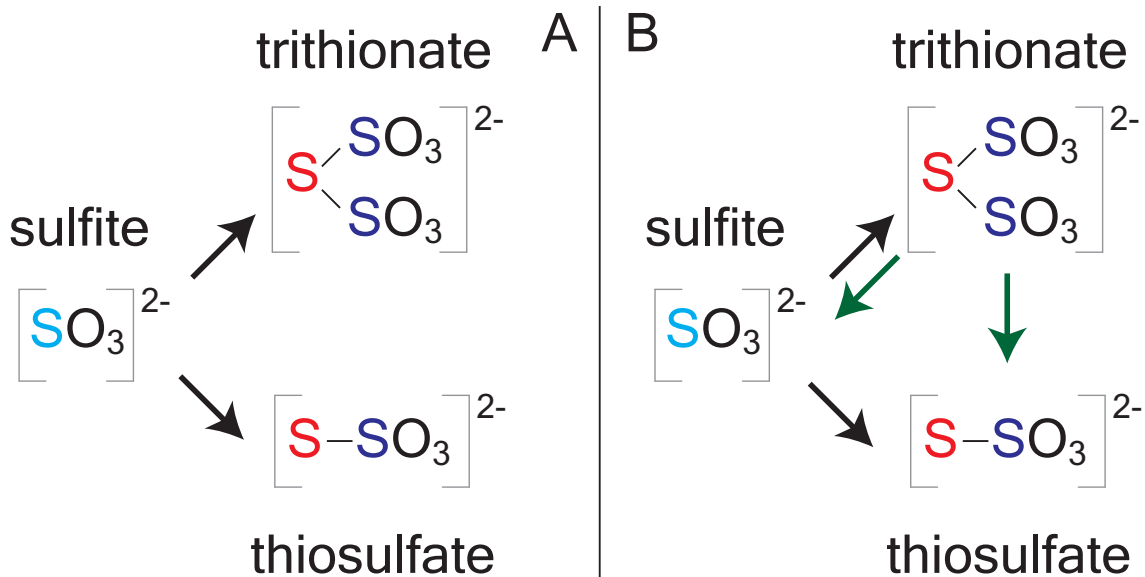
933   **Figure A4.** Reaction topology for closed-system models. (A) The simple model for early in the
934   experiments ($f > 0.85$). (B) Shows a more complex reaction model that may be applicable later in the
935   closed-system experiments ($f < 0.85$).

936

Leavitt, Bradley et al. 2015

937   **Figure A5.**
938
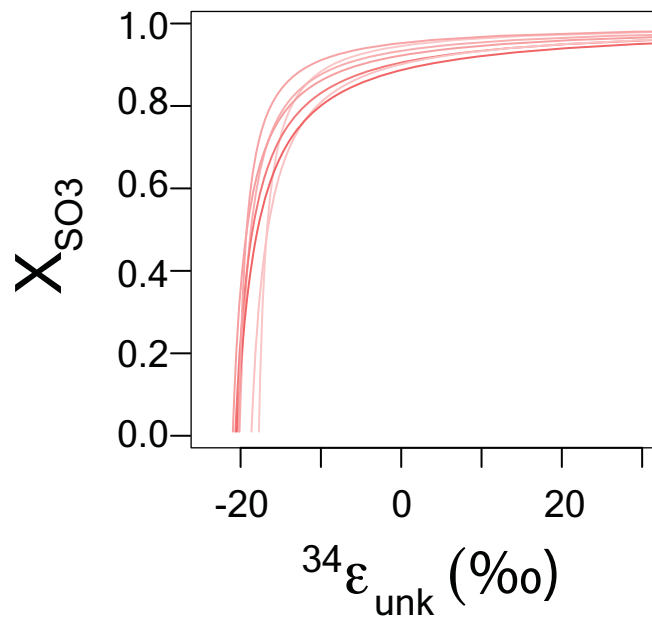
939
940
941   **Figure A5.** The relationship between the magnitude of a secondary fractionation ($^{34}\alpha_{secondary}$) and the
942   proportion of reduced sulfur deriving directly from sulfite reduction (X_{SO3}). The balance ($1\text{-}X_{SO3}$) is from
943   the parallel reduction of bound sulfonate. Errors estimates are from the propagation calculation,
944   incorporating both isotope and concentration analysis analytical errors (see below).
945
946

Leavitt, Bradley et al. 2015

947   **Figure A6**.
948
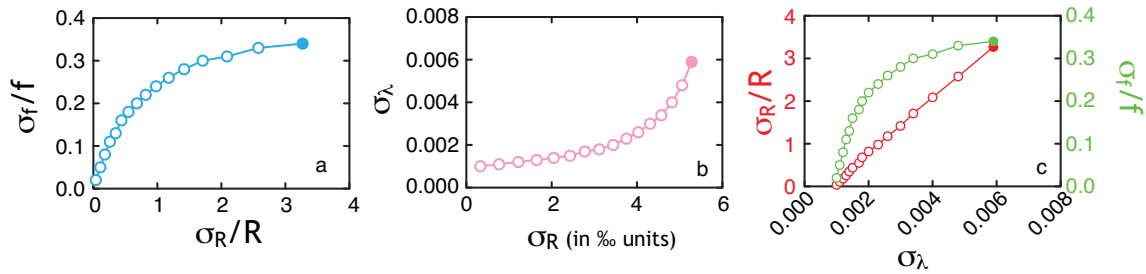
949
950   **Figure A6**. A series of frames (A-C) describing the origin and sensitivity of the controls on the resultant
951   error in $\delta^{34}S$ and $^{33}\lambda$ plotted in Figure A2 and 3. For this analysis, $^{34}\varepsilon$ is set to 15.3‰ to be consistent with
952   the reductive branch of the DsrAB experiments, the analytical precision of an isotope measurement is
953   0.2‰ in $\delta^{34}S$ and 0.008‰ in $\Delta^{33}S$, and f is allowed to vary from 0.6 to 0.9 in 0.02 increments (noted by
954   circles). This range in f is chosen to reflect the experimental range, and the circle is filled where $f =$
955   0.9. In (a), the covariance of the relative error in f (σ_f/f) is show to correlate with the error in the relative
956   isotope ratio, σ_R/R. As the calculated error in the R derived from the Rayleigh equation (σ_R) increases,
957   the consequence is an increase in the error in $^{33}\lambda$ (b). Finally, the relationship between the errors in both
958   f and R, as they contribute to the error on $^{33}\lambda$, are presented in frame c. Frames b and c do not approach
959   the origin as a result of f not approaching the limits of 0 and 1, and also due to the multivariate nature of
960   the propagation.
961
962

29

REFERENCES

Ames, D. P., and Willard, J. E. (1951). The Kinetics of the Exchange of Sulfur between Thiosulfate and Sulfite1. *J. Am. Chem. Soc.* 73, 164–172.

Antler, G., Turchyn, A. V., Rennie, V., Herut, B., and Sivan, O. (2013). Coupled sulfur and oxygen isotope insight into bacterial sulfate reduction in the natural environment. *Geochim Cosmochim Ac* 118, 98–117.

Bevington, P. R., and Robinson, D. K. (2003). Data reduction and error analysis. *McGraw–Hill, New York.*

Bigeleisen, J., and Wolfsberg, M. (1958). Theoretical and experimental aspects of isotope effects in chemical kinetics. *Advances in Chemical Physics, Volume 1*, 15–76.

Bolliger, C., Schroth, M. H., Bernasconi, S. M., Kleikemper, J., and Zeyer, J. (2001). Sulfur isotope fractionation during microbial sulfate reduction by toluene-degrading bacteria. *Geochim Cosmochim Ac* 65, 3289–3298.

Böttcher, M. E., Sievert, S. M., and Kuever, J. (1999). Fractionation of sulfur isotopes during dissimilatory reduction of sulfate by a thermophilic gram-negative bacterium at 60 C. *Arch Microbiol* 172, 125–128.

Bradford, M. M. (1976). A rapid and sensitive method for the quantitation of microgram quantities of protein utilizing the principle of protein-dye binding. *Analytical Biochemistry* 72, 248–254. doi:10.1016/0003-2697(76)90527-3.

Bradley, A. S., Leavitt, W. D., and Johnston, D. T. (2011). Revisiting the dissimilatory sulfate reduction pathway. *Geobiology* 9, 446–457. doi:10.1111/j.1472-4669.2011.00292.x.

Bradley, A. S., Leavitt, W. D., Schmidt, M. L., Knoll, A. H., Girguis, P. R., and Johnston, D. T. Physiological underpinnings of sulfur isotope fractionation during microbial sulfate reduction. *Geobiology*.

Bradley, A. S., Leavitt, W. D., Schmidt, M., Knoll, A. H., Girguis, P. R., and Johnston, D. T. (2015). Patterns of sulfur isotope fractionation during Microbial Sulfate Reduction. *Geobiology* in press. doi:10.1111/gbi.12149.

Brunner, B., and Bernasconi, S. M. (2005). A revised isotope fractionation model for dissimilatory sulfate reduction in sulfate reducing bacteria. *Geochim Cosmochim Ac* 69, 4759–4771.

Canfield, D. E. (2001a). Biogeochemistry of sulfur isotopes. *Reviews in Mineralogy and Geochemistry* 43, 607–636.

Canfield, D. E. (2001b). Isotope fractionation by natural populations of sulfate-reducing bacteria. *Geochim Cosmochim Ac* 65, 1117–1124.

Canfield, D. E. (2006). Models of oxic respiration, denitrification and sulfate reduction in zones of coastal upwelling. *Geochim Cosmochim Ac* 70, 5753–5765.

999   Canfield, D. E., and Farquhar, J. (2009). Animal evolution, bioturbation, and the sulfate concentration of
1000   the oceans. *Proceedings of the National Academy of Sciences* 106, 8123–8127.

1001   Canfield, D. E., Farquhar, J., and Zerkle, A. L. (2010). High isotope fractionations during sulfate
1002   reduction in a low-sulfate euxinic ocean analog. *Geol* 38, 415–418. doi:10.1130/G30723.1.

1003   Chambers, L. A., and Trudinger, P. A. (1975). Are thiosulfate and trithionate intermediates in
1004   dissimilatory sulfate reduction? *J Bacteriol* 123, 36–40.

1005   Chambers, L. A., and Trudinger, P. A. (1979). Microbiological fractionation of stable sulfur isotopes: a
1006   review and critique. *Geomicrobiology Journal* 1, 249–293.

1007   Chambers, L. A., Trudinger, P. A., Smith, J. W., and Burns, M. S. (1975). Fractionation of sulfur isotopes
1008   by continuous cultures of Desulfovibrio desulfuricans. *Can J Microbiol* 21, 1602–1607.

1009   Cline, J. D. (1969). Spectrophotometric determination of hydrogen sulfide in natural waters. *Limnol*
1010   *Oceanogr* 14, 454–458.

1011   Crowe, S., Paris, G., Katsev, S., Jones, C., Kim, S. T., Zerkle, A. L., Nomosatroyo, S., Fowle, D. A., Adkins,
1012   J. F., Sessions, A. L., et al. (2014). Sulfate was a trace constituent of Archean seawater. *Science* 346,
1013   735–739. doi:10.1126/science.1258966.

1014   Cypionka, H. (1994). Sulfate transport. *Methods in enzymology* 243, 3–14.

1015   Davidson, M. M., Bisher, M. E., Pratt, L. M., Fong, J., Southam, G., Pfiffner, S. M., Reches, Z., and
1016   Onstott, T. C. (2009). Sulfur Isotope Enrichment during Maintenance Metabolism in the
1017   Thermophilic Sulfate-Reducing Bacterium Desulfotomaculum putei. *Applied and Environmental*
1018   *Microbiology* 75, 5621–5630. doi:10.1128/AEM.02948-08.

1019   Detmers, J., Bruchert, V., Habicht, K., and Kuever, J. (2001). Diversity of sulfur isotope fractionations by
1020   sulfate-reducing prokaryotes. *Applied and Environmental Microbiology* 67, 888–894.

1021   Drake, H. L., and Akagi, J. M. (1977). Bisulfite reductase of Desulfovibrio vulgaris: explanation for
1022   product formation. *J Bacteriol* 132, 139–143.

1023   Drake, H. L., and Akagi, J. M. (1978). Dissimilatory reduction of bisulfite by Desulfovibrio vulgaris. *J*
1024   *Bacteriol* 136, 916–923.

1025   Drake, H. L., and Akagi, J. M. (1976). Product analysis of bisulfite reductase activity isolated from
1026   Desulfovibrio vulgaris. *J Bacteriol* 126, 733–738.

1027   Einsiedl, F. (2008). Effect of NO2− on stable isotope fractionation during bacterial sulfate reduction.
1028   *Environ Sci Technol* 43, 82–87.

1029   Farquhar, G. D., O'leary, M. H., and Berry, J. A. (1982). On the relationship between carbon isotope
1030   discrimination and the intercellular carbon dioxide concentration in leaves. *Functional Plant*
1031   *Biology* 9, 121–137.

1032   Farquhar, J., Canfield, D. E., Masterson, A., Bao, H., and Johnston, D. T. (2008). Sulfur and oxygen
1033   isotope study of sulfate reduction in experiments with natural populations from Faellestrand,

1034   Denmark. *Geochim Cosmochim Ac* 72, 2805–2821. doi:10.1016/j.gca.2008.03.013.

1035   Farquhar, J., Johnston, D. T., and Wing, B. A. (2007). Implications of conservation of mass effects on
1036   mass-dependent isotope fractionations: Influence of network structure on sulfur isotope phase space
1037   of dissimilatory sulfate reduction. *Geochim Cosmochim Ac* 71, 5862–5875.
1038   doi:10.1016/j.gca.2007.08.028.

1039   Farquhar, J., Johnston, D. T., Wing, B. A., Habicht, K. S., Canfield, D. E., Airieau, S., and Thiemens, M. H.
1040   (2003). Multiple sulphur isotopic interpretations of biosynthetic pathways: implications for
1041   biological signatures in the sulphur isotope record. *Geobiology* 1, 27–36.

1042   Ford, R. W. (1957). Sulphur isotope effects in chemical and biological processes. *PhD Thesis. McMaster*
1043   *University*.

1044   Fritz, G. (2002). Structure of adenylylsulfate reductase from the hyperthermophilic Archaeoglobus
1045   fulgidus at 1.6-A resolution. *Proceedings of the National Academy of Sciences* 99, 1836–1841.
1046   doi:10.1073/pnas.042664399.

1047   Fritz, P., Basharmal, G. M., Drimmie, R. J., and Ibsen, J. (1989). Oxygen isotope exchange between
1048   sulphate and water during bacterial reduction of sulphate. *Chemical Geology*.

1049   Furusaka, C. (1961). Sulphate Transport and Metabolism Desulphovibrio Desulphuricans. *Nature* 192,
1050   427–429.

1051   Garrels, R. M., and Lerman, A. (1981). Phanerozoic cycles of sedimentary carbon and sulfur. *P Natl*
1052   *Acad Sci Usa* 78, 4652–4656.

1053   Goldhaber, M. B., and Kaplan, I. R. (1975). Controls and consequences of sulfate reduction rates in
1054   recent marine sediments. *Soil Science* 119, 42–55.

1055   Gomes, M. L., and Hurtgen, M. T. (2015). Sulfur isotope fractionation in modern euxinic systems:
1056   Implications for paleoenvironmental reconstructionsof paired sulfate–sulfide isotope records.
1057   *Geochim Cosmochim Ac* 157, 39–55. doi:10.1016/j.gca.2015.02.031.

1058   Gomes, M. L., and Hurtgen, M. T. (2013). Sulfur isotope systematics of a euxinic, low-sulfate lake:
1059   Evaluating the importance of the reservoir effect in modern and ancient oceans. *Geol* 41, 663–666.
1060   doi:10.1130/G34187.1.

1061   Grant, W. M. (1947). Colorimetric determination of sulfur dioxide. *Anal. Chem.* 19, 345–346.

1062   Habicht, K. S., Salling, L., Thamdrup, B., and Canfield, D. E. (2005). Effect of Low Sulfate
1063   Concentrations on Lactate Oxidation and Isotope Fractionation during Sulfate Reduction by
1064   Archaeoglobus fulgidus Strain Z. *Applied and Environmental Microbiology* 71, 3770–3777.
1065   doi:10.1128/AEM.71.7.3770-3777.2005.

1066   Habicht, K., Gade, M., Thamdrup, B., Berg, P., and Canfield, D. E. (2002). Calibration of sulfate levels in
1067   the Archean Ocean. *Science* 298, 2372–2374.

1068   Harrison, A. G., and Thode, H. G. (1958). Mechanism of the bacterial reduction of sulphate from isotope
1069   fractionation studies. *Transactions of the Faraday Society* 54, 84–92.

1070 Harrison, A. G., and Thode, H. G. (1957). The kinetic isotope effect in the chemical reduction of
1071   sulphate. *Transactions of the Faraday Society* 53, 1648–1651.

1072 Hayes, J. M. (1993). Factors controlling 13 C contents of sedimentary organic compounds: Principles
1073   and evidence. *Marine Geology* 113, 111–125.

1074 Hayes, J. M. (2001). Fractionation of carbon and hydrogen isotopes in biosynthetic processes. *Reviews*
1075   *in Mineralogy and Geochemistry* 43, 225–277.

1076 Hayes, J. M. (1983). Practice and principles of isotopic measurements in organic geochemistry. *Organic*
1077   *Geochemistry of Contemporaneous and Ancient Sediments*, 5–31.

1078 Hayes, J. M., Strauss, H., and Kaufman, A. J. (1999). The abundance of 13C in marine organic matter and
1079   isotopic fractionation in the global biogeochemical cycle of carbon during the past 800 Ma.
1080   *Chemical Geology* 161, 103–125.

1081 Hoek, J., Reysenbach, A.-L., Habicht, K., and Canfield, D. (2006). Effect of hydrogen limitation and
1082   temperature on the fractionation of sulfur isotopes by a deep-sea hydrothermal vent sulfate-reducing
1083   bacterium. *Geochim Cosmochim Ac* 70, 5831–5841. doi:10.1016/j.gca.2006.07.031.

1084 Holland, H. D. (1973). Systematics of the isotopic composition of sulfur in the oceans during the
1085   Phanerozoic and its implications for atmospheric oxygen. *Geochim Cosmochim Ac* 37, 2605–2616.

1086 Holler, T., Wegener, G., Niemann, H., Deusner, C., Ferdelman, T. G., Boetius, A., Brunner, B., and
1087   Widdel, F. (2011). Carbon and sulfur back flux during anaerobic microbial oxidation of methane
1088   and coupled sulfate reduction. *Proceedings of the National Academy of Sciences* 108, E1484–
1089   E1490. doi:10.1073/pnas.1106032108/-/DCSupplemental.

1090 Johnston, D. T. (2005). Multiple sulfur isotope fractionations in biological systems: A case study with
1091   sulfate reducers and sulfur disproportionators. *Am J Sci* 305, 645–660. doi:10.2475/ajs.305.6-8.645.

1092 Johnston, D. T., Farquhar, J., and Canfield, D. E. (2007). Sulfur isotope insights into microbial sulfate
1093   reduction: When microbes meet models. *Geochim Cosmochim Ac* 71, 3929–3947.
1094   doi:10.1016/j.gca.2007.05.008.

1095 Jones, G. E., and Starkey, R. L. (1957). Fractionation of Stable Isotopes of Sulfur by Microorganisms and
1096   Their Role in Deposition of Native Sulfur. *Applied Microbiology* 5, 111.

1097 Kaplan, I. R., and Rittenberg, S. C. (1964). Microbiological fractionation of sulphur isotopes. *Journal of*
1098   *General Microbiology* 34, 195–212.

1099 Karkhoff-Schweizer, R. R., Bruschi, M., and Voordouw, G. (1993). Expression of the gamma-subunit
1100   gene of desulfoviridin-type dissimilatory sulfite reductase and of the alpha- and beta-subunit genes is
1101   not coordinately regulated. *Eur J Biochem* 211, 501–507. doi:10.1111/j.1432-1033.1993.tb17576.x.

1102 Karsh, K. L., Granger, J., Kritee, K., and Sigman, D. M. (2012). Eukaryotic Assimilatory Nitrate
1103   Reductase Fractionates N and O Isotopes with a Ratio near Unity. *Environ Sci Technol* 46, 5727–
1104   5735. doi:10.1021/es204593q.

1105 Kelly, D. P., and Wood, A. P. (1994). [35] Synthesis and determination of thiosulfate and polythionates.

1106   *Methods in enzymology* 243, 475–501.

1107   Kelly, D. P., Chambers, L. A., and Trudinger, P. A. (1969). Cyanolysis and spectrophotometric
1108   estimation of trithionate in mixture with thiosulfate and tetrathionate. *Anal. Chem.* 41, 898–901.

1109   Kemp, A., and Thode, H. G. (1968). The mechanism of the bacterial reduction of sulphate and of
1110   sulphite from isotope fractionation studies. *Geochim Cosmochim Ac* 32, 71–91.

1111   Kim, J. H., and Akagi, J. M. (1985). Characterization of a trithionate reductase system from Desulfovibrio
1112   vulgaris. *J Bacteriol* 163, 472–475.

1113   Kleikemper, J., Schroth, M., Bernasconi, S. M., Brunner, B., and Zeyer, J. (2004). Sulfur isotope
1114   fractionation during growth of sulfate-reducing bacteria on various carbon sources. *Geochim*
1115   *Cosmochim Ac* 68, 4891–4904. doi:10.1016/j.gca.2004.05.034.

1116   Knöller, K., Vogt, C., Richnow, H.-H., and Weise, S. M. (2006). Sulfur and Oxygen Isotope Fractionation
1117   during Benzene, Toluene, Ethyl Benzene, and Xylene Degradation by Sulfate-Reducing Bacteria.
1118   *Environ Sci Technol* 40, 3879–3885. doi:10.1021/es052325r.

1119   Kobayashi, K., Yasuhide, S., and Ishimoto, M. (1974). Biochemical Studies on Sulfate-reducing Bacteria
1120   XIII. Sulfite Reductase fromDesulfovibrio vulgaris-Mechanism of Trithionafe, Thiosulfate, and
1121   Sulfide Formation and Enzymatic Properties. *Journal of biochemistry* 75, 519–529.

1122   Krouse, H. R., McCready, R. G. L., Husain, S. A., and Campbell, J. N. (1968). Sulfur Isotope
1123   Fractionation and Kinetic Studies of Sulfite Reduction in Growing Cells of Salmonella heidelberg.
1124   *Biophysical Journal* 8, 109–124. doi:10.1016/S0006-3495(68)86478-1.

1125   Laws, E. A., Popp, B. N., Bidigare, R. R., Kennicutt, M. C., and Macko, S. A. (1995). Dependence of
1126   phytoplankton carbon isotopic composition on growth rate and [CO 2) aq: Theoretical
1127   considerations and experimental results. *Geochim Cosmochim Ac* 59, 1131–1138.

1128   Le Gall, J., Payne, W. J., Chen, L., Liu, M. Y., and Xavier, A. V. (1994). Localization and specificity of
1129   cytochromes and other electron transfer proteins from sulfate-reducing bacteria. *Biochimie* 76, 655–
1130   665.

1131   Leavitt, W. D. (2014). On the mechanisms of sulfur isotope fractionation during microbial sulfate
1132   reduction. *PhD Thesis. Harvard University.*

1133   Leavitt, W. D., Cummins, R., Schmidt, M. L., Sim, M. S., Ono, S., Bradley, A. S., and Johnston, D. T.
1134   (2014). Multiple sulfur isotope signatures of sulfite and thiosulfate reduction by the model
1135   dissimilatory sulfate-reducer, Desulfovibrio alaskensis str. G20. *Frontiers in Microbiology* 5.

1136   Leavitt, W. D., Halevy, I., Bradley, A. S., and Johnston, D. T. (2013). Influence of sulfate reduction rates
1137   on the Phanerozoic sulfur isotope record. *P Natl Acad Sci Usa* 110, 11244–11249.
1138   doi:10.1073/pnas.1218874110.

1139   Mangalo, M., Einsiedl, F., Meckenstock, R. U., and Stichler, W. (2008). Influence of the enzyme
1140   dissimilatory sulfite reductase on stable isotope fractionation during sulfate reduction. *Geochim*
1141   *Cosmochim Ac* 72, 1513–1520. doi:10.1016/j.gca.2008.01.006.

1142 Mangalo, M., Meckenstock, R. U., Stichler, W., and Einsiedl, F. (2007). Stable isotope fractionation
1143 during bacterial sulfate reduction is controlled by reoxidation of intermediates. *Geochim*
1144 *Cosmochim Ac* 71, 4161–4171. doi:10.1016/j.gca.2007.06.058.

1145 Mariotti, A., Germon, J. C., Hubert, P., Kaiser, P., Letolle, R., Tardieux, A., and Tardieux, P. (1981).
1146 Experimental determination of nitrogen kinetic isotope fractionation: Some principles; illustration
1147 for the denitrification and nitrification processes. *Plant Soil* 62, 413–430.
1148 doi:10.1007/BF02374138.

1149 Marritt, S. J., and Hagen, W. R. (1996). Dissimilatory Sulfite Reductase Revisited. The Desulfoviridin
1150 Molecule does Contain 20 Iron Ions, Extensively Demetallated Sirohaem, and an S= 9/2 Iron-Sulfur
1151 Cluster. *Eur J Biochem* 238, 724–727. doi:10.1111/j.1432-1033.1996.0724w.x.

1152 McCready, R. G. L. (1975). Sulfur Isotope Fractionation by Desulfovibrio and Desulfotomaculum
1153 species. *Geochim Cosmochim Ac* 39, 1395–1401.

1154 McCready, R. G. L., Laishley, E. J., and Krouse, H. R. (1975). Stable isotope fractionation by Clostridium
1155 pasteurianum. 1.34 S/32S: inverse isotope effects during SO42-and SO32-reduction. *Can J*
1156 *Microbiol* 21, 235–244.

1157 McNaught, A. D., and Wilkinson, A. (1997). International Union of Pure and Applied Chemistry.

1158 Miller, M. F. (2002). Isotopic fractionation and the quantification of 17 O anomalies in the oxygen three-
1159 isotope system: an appraisal and geochemical significance. *Geochim Cosmochim Ac* 66, 1881–1889.

1160 Nakagawa, M., Ueno, Y., Hattori, S., Umemura, M., Yagi, A., Takai, K., Koba, K., Sasaki, Y., Makabe, A.,
1161 and Yoshida, N. (2012). Seasonal change in microbial sulfur cycling in monomictic Lake Fukami-
1162 ike, Japan. *Limnol Oceanogr* 57, 974–988. doi:10.4319/lo.2012.57.4.0974.

1163 Nakai, N., and Jensen, M. L. (1964). The kinetic isotope effect in the bacterial reduction and oxidation of
1164 sulfur. *Geochim Cosmochim Ac* 28, 1893–1912. doi:10.1016/0016-7037(64)90136-X.

1165 Newton, G. L., Dorian, R., and Fahey, R. C. (1981). Analysis of biological thiols: derivatization with
1166 monobromobimane and separation by reverse-phase high-performance liquid chromatography.
1167 *Analytical Biochemistry* 114, 383–387.

1168 Oliveira, T. F., Franklin, E., Afonso, J. P., Khan, A. R., Oldham, N. J., Pereira, I. A. C., and Archer, M.
1169 (2011). Structural Insights into Dissimilatory Sulfite Reductases: Structure of Desulforubidin from
1170 Desulfomicrobium Norvegicum. *Frontiers in Microbiology* 2. doi:10.3389/fmicb.2011.00071.

1171 Oliveira, T. F., Vonrhein, C., Matias, P. M., Venceslau, S. S., Pereira, I. A. C., and Archer, M. (2008a).
1172 Purification, crystallization and preliminary crystallographic analysis of a dissimilatory DsrAB sulfite
1173 reductase in complex with DsrC. *J Struct Biol* 164, 236–239. doi:10.1016/j.jsb.2008.07.007.

1174 Oliveira, T. F., Vonrhein, C., Matias, P. M., Venceslau, S. S., Pereira, P. M., and Archer, M. (2008b). The
1175 crystal structure of Desulfovibrio vulgaris dissimilatory sulfite reductase bound to DsrC provides
1176 novel insights into the mechanism of sulfate respiration. *J Biol Chem* 283, 34141–34149.
1177 doi:10.1074/jbc.M805643200.

1178 Pagani, M., Liu, Z., LaRiviere, J., and Ravelo, A. C. (2009). High Earth-system climate sensitivity

1179   determined from Pliocene carbon dioxide concentrations. *Nature Geosci* 3, 27–30.
1180   doi:10.1038/ngeo724.

1181   Pallud, C., Meile, C., Laverman, A. M., Abell, J., and Van Cappellen, P. (2007). The use of flow-through
1182   sediment reactors in biogeochemical kinetics: methodology and examples of applications. *Marine*
1183   *Chemistry* 106, 256–271.

1184   Parey, K., Fritz, G., Ermler, U., and Kroneck, P. M. H. (2013). Conserving energy with sulfate around
1185   100 °C – structure and mechanism of key metal enzymes in hyperthermophilic Archaeoglobus
1186   fulgidus. *Metallomics* 5, 302. doi:10.1039/c2mt20225e.

1187   Parey, K., Warkentin, E., Kroneck, P. M., and Ermler, U. (2010). Reaction cycle of the dissimilatory
1188   sulfite reductase from Archaeoglobus fulgidus. *Biochemistry* 49, 8912–8921.
1189   doi:10.1021/bi100781f.

1190   Park, R., and Epstein, S. (1960). Carbon isotope fractionation during photosynthesis. *Geochim*
1191   *Cosmochim Ac* 21, 110–126.

1192   Peck, H. D. (1961). Enzymatic basis for assimilatory and dissimilatory sulfate reduction. *J Bacteriol* 82,
1193   933–939.

1194   Peck, H. D. (1962). The role of adenosine-5'-phosphosulfate in the reduction of sulfate to sulfite by
1195   Desulfovibrio desulfuricans. *J Biol Chem* 237, 198–203.

1196   Peck, H. D., Jr (1959). The ATP-dependent reduction of sulfate with hydrogen in extracts of
1197   Desulfovibrio desulfuricans. *P Natl Acad Sci Usa* 45, 701.

1198   Peck, H. D., Jr. (1960). Adenosine 5′-Phosphosulphate as an intermediate in the oxidation of thiosulfate
1199   by Thiobacillus thioparus. *P Natl Acad Sci Usa* 46, 1053.

1200   Pereira, I. A. C., Ramos, A. R., Grein, F., Marques, M. C., Da Silva, S. M., and Venceslau, S. S. (2011). A
1201   comparative genomic analysis of energy metabolism in sulfate reducing bacteria and archaea.
1202   *Frontiers in Microbiology* 2. doi:10.3389/fmicb.2011.00069.

1203   Pires, R. H., Lourenço, A. I., Morais, F., Teixeira, M., Xavier, A. V., Saraiva, L. M., and Pereira, I. A. C.
1204   (2003). A novel membrane-bound respiratory complex from Desulfovibrio desulfuricans ATCC
1205   27774. *Biochimica et Biophysica Acta (BBA) - Bioenergetics* 1605, 67–82. doi:10.1016/S0005-
1206   2728(03)00065-3.

1207   Piłsyk, S., and Paszewski, A. (2009). Sulfate permeases — phylogenetic diversity of sulfate transport.
1208   *Acta Biocimica Polonica* 56, 375–384.

1209   Price, M. N., Ray, J., Wetmore, K. M., Kuehl, J. V., Bauer, S., Deutschbauer, A. M., and Arkin, A. P.
1210   (2014). The genetic basis of energy conservation in the sulfate-reducing bacterium Desulfovibrio
1211   alaskensis G20. *Frontiers in Microbiology* 5.

1212   Rees, C. (1973). A steady-state model for sulphur isotope fractionation in bacterial reduction processes.
1213   *Geochim Cosmochim Ac* 37, 1141–1162.

1214   Romão, C. V., Pereira, I. A. C., Xavier, A. V., LeGall, J., and Teixeira, M. (1997). Characterization of the

1215 [NiFe] Hydrogenase from the Sulfate ReducerDesulfovibrio vulgarisHildenborough. *Biochemical*
1216 *and Biophysical Research Communications* 240, 75–79. doi:10.1006/bbrc.1997.7598.

1217 Sass, H., Steuber, J., Kroder, M., Kroneck, P., and Cypionka, H. (1992). Formation of thionates by
1218 freshwater and marine strains of sulfate-reducing bacteria. *Arch Microbiol* 158, 418–421.

1219 Scheller, S., Goenrich, M., Thauer, R. K., and Jaun, B. (2013). Methyl-Coenzyme M Reductase from
1220 Methanogenic Archaea: Isotope Effects on the Formation and Anaerobic Oxidation of Methane. *J.*
1221 *Am. Chem. Soc.* 135, 14975–14984. doi:10.1021/ja406485z.

1222 Schiffer, A., Parey, K., Warkentin, E., Diederichs, K., Huber, H., Stetter, K. O., Kroneck, P. M., and
1223 Ermler, U. (2008). Structure of the Dissimilatory Sulfite Reductase from the Hyperthermophilic
1224 Archaeon Archaeoglobus fulgidus. *Journal of Molecular Biology* 379, 1063–1074.

1225 Sim, M. S., Bosak, T., and Ono, S. (2011a). Large Sulfur Isotope Fractionation Does Not Require
1226 Disproportionation. *Science* 333, 74–77. doi:10.1126/science.1205103.

1227 Sim, M. S., Ono, S., and Bosak, T. (2012). Effects of Iron and Nitrogen Limitation on Sulfur Isotope
1228 Fractionation during Microbial Sulfate Reduction. *Applied and Environmental Microbiology* 78,
1229 8368–8376. doi:10.1128/AEM.01842-12.

1230 Sim, M. S., Ono, S., Donovan, K., Templer, S. P., and Bosak, T. (2011b). Effect of electron donors on the
1231 fractionation of sulfur isotopes by a marine Desulfovibrio sp. *Geochim Cosmochim Ac*, 1–16.
1232 doi:10.1016/j.gca.2011.05.021.

1233 Sim, M. S., Wang, D. T., Zane, G. M., Wall, J. D., Bosak, T., and Ono, S. (2013). Fractionation of sulfur
1234 isotopes by Desulfovibrio vulgaris mutants lacking hydrogenases or type I tetraheme cytochrome c3.
1235 *Frontiers in Microbiology* 4.

1236 Smock, A., Bottcher, M., and Cypionka, H. (1998). Fractionation of sulfur isotopes during thiosulfate
1237 reduction by Desulfovibrio desulfuricans. *Arch Microbiol* 169, 460–463.

1238 Soriano, A., and Cowan, J. A. (1995). Sulfite Reductase: Active Site Residues are "Noncatalytic."
1239 Comparison of Reaction Energetics for Enzyme- and Siroheme-Catalyzed Reduction of Inorganic
1240 Substrates. *J. Am. Chem. Soc.* 117, 4724–4725. doi:10.1021/ja00121a038.

1241 Sörbo, B. O. (1957). A colorimetric method for the determination of thiosulfate. *Biochimica et*
1242 *Biophysica acta* 23, 412–416.

1243 Sra, A. K., Hu, Y., Martin, G. E., Snow, D. D., Ribbe, M. W., and Kohen, A. (2004). Competitive 15N
1244 Kinetic Isotope Effects of Nitrogenase-Catalyzed Dinitrogen Reduction. *J. Am. Chem. Soc.* 126,
1245 12768–12769. doi:10.1021/ja0458470.

1246 Suh, B., and Akagi, J. M. (1969). Formation of Thiosulfate from Sulfite by Desulfovibrio vulgaris. *J*
1247 *Bacteriol.*

1248 Tcherkez, G. G. B., Farquhar, G. D., and Andrews, T. J. (2006). Despite slow catalysis and confused
1249 substrate specificity, all ribulose bisphosphate carboxylases may be nearly perfectly optimized. *P*
1250 *Natl Acad Sci Usa* 103, 7246–7251. doi:10.1073/pnas.0600605103.

1251   Thode, H. G., Kleerekoper, H., and McElcheran, D. (1951). Isotope fractionation in the bacteria
1252   reduction of sulfate. *Research (London)* 4, 581–582.

1253   Thode, H. G., Monster, J., and Dunford, H. B. (1961). Sulphur Isotope Geochemistry. *Geochim*
1254   *Cosmochim Ac* 25, 159–174.

1255   Tudge, A. P., and Thode, H. G. (1950). Thermodynamic properties of isotopic compounds of sulphur.
1256   *Canadian Journal of Research* 28, 567–578.

1257   Turchyn, A. V., Brüchert, V., Lyons, T. W., Engel, G. S., Balci, N., Schrag, D. P., and Brunner, B. (2010).
1258   Kinetic oxygen isotope effects during dissimilatory sulfate reduction: a combined theoretical and
1259   experimental approach. *Geochim Cosmochim Ac* 74, 2011–2024. doi:10.1016/j.gca.2010.01.004.

1260   Vairavamurthy, A., Manowitz, B., Luther Iii, G. W., and Jeon, Y. (1993). Oxidation state of sulfur in
1261   thiosulfate and implications for anaerobic energy metabolism. *Geochim Cosmochim Ac* 57, 1619–
1262   1623.

1263   Venceslau, S. S., Cort, J. R., Baker, E. S., Chu, R. K., Robinson, E. W., Dahl, C., Saraiva, L. M., and Pereira,
1264   I. A. (2013). Redox states of Desulfovibrio vulgaris DsrC, a key protein in dissimilatory sulfite
1265   reduction. *Biochemical and Biophysical Research Communications* 441, 732–736.

1266   Venceslau, S. S., Stockdreher, Y., Dahl, C., and Pereira, I. A. C. (2014). The "bacterial heterodisulfide"
1267   DsrC is a key protein in dissimilatory sulfur metabolism. *Biochimica et Biophysica Acta (BBA) -*
1268   *Bioenergetics* 1837, 1148–1164. doi:10.1016/j.bbabio.2014.03.007.

1269   Wing, B. A., and Halevy, I. (2014). Intracellular metabolite levels shape sulfur isotope fractionation
1270   during microbial sulfate respiration. *P Natl Acad Sci Usa*. doi:10.1073/pnas.1407502111.

1271   Wolfe, B. M., Lui, S. M., and Cowan, D. (1994). Desulfoviridin, a multimeric-dissimilatory sulfite
1272   reductase from Desulfovibrio vulgaris (Hildenborough) Purification, characterization, kinetics and
1273   EPR studies. *Eur J Biochem* 223, 79–89. doi:10.1111/j.1432-1033.1994.tb18968.x.

1274   Young, E. D., Galy, A., and Nagahara, H. (2002). Kinetic and equilibrium mass-dependent isotope
1275   fractionation laws in nature and their geochemical and cosmochemical significance. *Geochim*
1276   *Cosmochim Ac* 66, 1095–1104.

1277